



Can sampling biases explain the discrepancies between lower stratospheric water vapour trend estimates derived from the FPH observations at Boulder and a merged zonal mean satellite data set?

Stefan Lossow¹, Dale F. Hurst², Karen H. Rosenlof², Gabriele P. Stiller¹, Thomas von Clarmann¹, Sabine Brinkop³, Martin Dameris³, Patrick Jöckel³, Doug E. Kinnison⁴, Johannes Plieninger¹, David A. Plummer⁵, Felix Ploeger⁶, William G. Read⁷, Ellis E. Remsberg⁸, James M. Russell⁹, and Mengchu Tao⁶

¹Karlsruhe Institute of Technology, Institute for Meteorology and Climate Research, Hermann-von-Helmholtz-Platz 1, 76344 Leopoldshafen, Germany.

²NOAA Earth System Research Laboratory, Global Monitoring Division, 325 Broadway, Boulder, CO 80305, USA.

³Deutsches Zentrum für Luft- und Raumfahrt (DLR), Institut für Physik der Atmosphäre, 82234 Oberpfaffenhofen-Wessling, Germany.

⁴University of Colorado, Atmospheric Chemistry Observations & Modeling Laboratory, P.O. Box 3000, Boulder, CO 80305-3000, USA.

⁵Environment and Climate Change Canada, Climate Research Branch, 550 Sherbrooke ouest, Montréal, Quebec H3A 1B9, Canada.

⁶Forschungszentrum Jülich, Institute for Energy and Climate Research: Stratosphere (IEK-7), Leo-Brandt-Straße, 52425 Jülich, Germany.

⁷Jet Propulsion Laboratory, 4800 Oak Grove Drive, Pasadena, CA 91109, USA.

⁸NASA Langley Research Center, 21 Langley Boulevard, Hampton, VA 23681, USA.

⁹Hampton University, Center for Atmospheric Sciences, 23 Tyler Street Hampton, VA 23668, USA.

Correspondence to: Stefan Lossow (stefan.lossow@kit.edu)

1
2
3 **Abstract.** Trend estimates with different signs are reported in the literature for lower stratospheric water vapour considering the
4 time period between the late 1980s and 2010. The NOAA (National Oceanic and Atmospheric Administration) frost point hy-
5 grometer (FPH) observations at Boulder (Colorado, 40.0°N, 105.2°W) indicate positive trends (about 0.12 ppmv · decade⁻¹ –
6 0.45 ppmv · decade⁻¹). Contrary, negative trends (approximately –0.15 ppmv · decade⁻¹ – –0.05 ppmv · decade⁻¹) are de-
7 rived from a merged zonal mean satellite data set for a latitude band around the Boulder latitude. Overall, the trend differ-
8 ences between the two data sets range from about 0.25 ppmv · decade⁻¹ to 0.45 ppmv · decade⁻¹, depending on altitude.
9 It has been proposed that a possible explanation for these discrepancies is a different temporal behaviour at Boulder and
10 the zonal mean, which simply indicates a sampling bias. In this work we investigate trend differences between Boulder and
11 the zonal mean using primarily simulations from ECHAM/MESSy (European Centre for Medium-Range Weather Forecasts
12 Hamburg/Modular Earth Submodel System) Atmospheric Chemistry (EMAC), WACCM (Whole Atmosphere Community Cli-
13 mate Model), CMAM (Canadian Middle Atmosphere Model) and CLaMS (Chemical Lagrangian Model of the Stratosphere).
14 On shorter time scales we address this aspect also based on satellite observations from UARS/HALOE (Upper Atmosphere



1 Research Satellite/Halogen Occultation Experiment), Envisat/MIPAS (Environmental Satellite/Michelson Interferometer for
2 Passive Atmospheric Sounding) and Aura/MLS (Microwave Limb Sounder). Overall, both the simulations and observations
3 exhibit trend differences between Boulder and the zonal mean. The differences are dependent on altitude and the time period
4 considered. The model simulations indicate only small trend differences between Boulder and the zonal mean for the time
5 period between the late 1980s and 2010. These are clearly not sufficient to explain the discrepancies between the trend esti-
6 mates derived from the FPH observations and the merged zonal mean satellite data set. Unless the simulations underrepresent
7 variability or the trend differences originate from smaller spatial and temporal scales than resolved by the model simulations,
8 trends at Boulder for this time period should be quite representative also for the zonal mean and even other latitude bands.
9 Trend differences for a decade of data are larger and need to be kept in mind when comparing results for Boulder and the zonal
10 mean on this time scale. Beyond that, we find that the trend estimates for the time period between the late 1980s and 2010 also
11 significantly differ among the simulations. They are larger than those derived from the merged satellite data set and smaller
12 than the trend estimates derived from the FPH observations.

13 1 Introduction

14 Water vapour in the stratosphere plays a fundamental role in the radiative budget and affects the ozone chemistry in this
15 atmospheric layer. In the lower stratosphere water vapour is the most important greenhouse gas. As such, it is part of an
16 important global warming feedback mechanism. A warmer climate increases lower stratospheric water vapour, leading to an
17 even warmer climate. Dessler et al. (2013) estimated this feedback to be $0.3 \text{ W} \cdot \text{m}^{-2}$ for a temperature anomaly of 1 K at
18 500 hPa. Besides that, water vapour is a fundamental component of polar stratospheric clouds. The heterogeneous chemistry
19 on cloud particle surfaces is responsible for the severe ozone depletion in the lower stratosphere during winter and spring,
20 especially in the Antarctic (Solomon, 1999). Water vapour is also the main source of hydrogen radicals ($\text{HO}_x = \text{OH}, \text{H}, \text{HO}_2$)
21 in the stratosphere that contribute to ozone destruction through catalytic loss cycles (Brasseur and Solomon, 2005).

22 Thus, any change of stratospheric water vapour over a longer time scale has important implications (e.g. Dvortsov and
23 Solomon, 2001; Forster and Shine, 2002; Stenke and Grewe, 2005; Solomon et al., 2010; Riese et al., 2012; Maycock et al.,
24 2014; Gilford et al., 2016). In the past, the majority of studies related to longer term water vapour changes were based on
25 observations by the balloon-borne NOAA frost point hygrometer at Boulder (a more detailed description of the measurement
26 principle is provided in Sect. 2.2.4). These observations have been performed since 1980, typically once per month, providing
27 the longest time series of water vapour in the lower stratosphere. Positive trends over Boulder were first reported by Oltmans
28 and Hofmann (1995), then by Oltmans et al. (2000), Scherer et al. (2008) and finally Hurst et al. (2011). For the time period
29 from 1980 to 2010, Hurst et al. (2011) showed an overall increase of $0.24 \text{ ppmv} \cdot \text{decade}^{-1}$ to $0.42 \text{ ppmv} \cdot \text{decade}^{-1}$ for the
30 altitude range between 16 km and 26 km accompanied by significant variability on shorter time scales. 25% of the observed
31 increase could be associated to changes of methane (Hurst et al., 2011). The oxidation of this trace gas is the most important in
32 situ source of water vapour in the stratosphere. The other relevant source of water vapour in the stratosphere is transport from the
33 troposphere, which mainly occurs through the cold tropical tropopause region. One major pathway is slow ascent (accompanied



1 by large horizontal motions, Holton and Gettelman, 2001) where the amount of water vapour entering the stratosphere is mainly
2 controlled by the tropopause temperature (or better cold point temperature, Fueglistaler et al., 2009). Different changes of this
3 temperature have been reported. Rosenlof and Reid (2008) reported an overall negative trend for the time period from 1980
4 to 2003, which would correspondingly result in a decrease of lower stratospheric water vapour. Recent work by Randel et al.
5 (2017) indicates zero or slightly positive trends at the tropical tropopause for the time periods 1979 to 1997 and 1998 to 2014.
6 The other pathway thought to be of importance is the convective lofting of ice particles (Moyer et al., 1996; Dessler et al.,
7 2016; Avery et al., 2017). Once the particles reach the stratosphere, they evaporate and enhance the amount of stratospheric
8 water vapour. This process is not dependent on the (cold point) temperature. Balloon-borne observations indicated no trend
9 of the convective ice lofting into the stratosphere for the time period between 1991 and 2007 (Notholt et al., 2010). Based on
10 all these results it is difficult to assess what process(es) caused the 30 year net increase of lower stratospheric water vapour
11 observed by the FPH observations at Boulder (Hurst et al., 2011).

12 Satellite observations of stratospheric water vapour exist since 1978 (Gille and Russell, 1984), with some gaps. The instru-
13 ments have limited life times and thus individual data sets do not allow a trend analysis on the same time scale as the FPH
14 observations at Boulder. Recently, Hegglin et al. (2014) merged zonal mean data sets from seven satellite instruments. This
15 merging was achieved with help of CMAM simulations with specified dynamics (aka nudging) which acted as a transfer func-
16 tion. For each data set biases relative to the CMAM simulations were estimated. This assumes that the CMAM simulations pro-
17 vide a realistic representation of the water vapour variability (including trends) and that the satellite data sets do not have a drift
18 in the bias estimation period. With this bias information the individual data sets were then adjusted relative to the Aura/MLS
19 observations. Finally the average over all bias-corrected data sets was used for the merged data set. This data set covers the time
20 period between 1986 or 1988 (depending on latitude and altitude) and 2010, providing the opportunity to evaluate the trends
21 observed by the FPH observations at Boulder and to address water vapour changes on a more global scale. The trends derived
22 from the merged satellite data set for the zonal mean of the latitude around Boulder were negative below about 10 hPa and
23 positive above. This behaviour could be essentially also observed at all other latitudes. Below 20 hPa the percentage changes
24 up to 2010 were typically between -5% to -10% , which roughly corresponds to a trend between $-0.05 \text{ ppmv} \cdot \text{decade}^{-1}$ and
25 $-0.15 \text{ ppmv} \cdot \text{decade}^{-1}$. Hegglin et al. (2014) attributed this trend to a reduced transport of water vapour into the stratosphere
26 as a consequence of lower tropopause temperatures and a changed circulation in the stratosphere. During the same period as
27 covered by the merged satellite data set, the FPH observations at Boulder still exhibit a clear increase of lower stratospheric
28 water vapour (Hurst et al., 2011).

29 Figure 1 provides a summary of the trend discrepancies between the FPH observations and the merged satellite data. The
30 trends derived from the merged satellite data set for the latitude band around Boulder ($35^\circ\text{N} - 45^\circ\text{N}$) are shown in green.
31 Below (above) the dashed line the satellite trends are representative for the time period from 1988 to 2010 (1986 to 2010).
32 The estimates are based on a digitisation of Fig. 5a in Hegglin et al. (2014). The extracted percentage trends were converted
33 to volume mixing ratio trends by assuming a constant reference mixing ratio of 3 ppmv. Consequently, the trends presented in
34 Fig. 1 are approximations. They are likely an underestimate as the actual reference mixing ratio is probably somewhat larger.
1 We know that the trends are at least statistically significant at the 2σ uncertainty level, but the actual level is unknown to us. As



2 a conservative estimate we assume that the uncertainty is exactly at the 2σ level, consequently overestimating the actual trend
3 uncertainties. In red (blue) the trends derived from the FPH observations at Boulder are given for the time period from 1986
4 to 2010 (1988 to 2010). These were obtained by means of multi-linear regressions (see Eq. 2 later). Only small differences are
5 observed between two time periods. The trend estimates do not change significantly if the vertical resolution of the FPH data is
6 adjusted to that of the satellite observations. Likewise smoothing the FPH observations in time (with a 1 year running average),
7 to reduce the scatter among individual observations, does not notably affect the trend estimates.

8 The lower panel of Fig. 1 shows an estimate of the differences in the trend estimates between the FPH observations and
9 the merged zonal mean satellite data set. The differences vary with altitude ranging from about $0.25 \text{ ppmv} \cdot \text{decade}^{-1}$ to
10 $0.45 \text{ ppmv} \cdot \text{decade}^{-1}$. As argued above, the absolute size is probably underestimated while uncertainties are overestimated.
11 Given the importance of water vapour in the lower stratosphere there is a dire need to reconcile these differences. Potential
12 explanations could be the following or a combination of these:

- 13 (1) There might be problems with one data set or even with both.
- 14 (2) The location of Boulder might be not representative for the zonal mean due to, e.g. local processes specific for the location
15 (American monsoon, lee side of the Rocky Mountains etc.)
- 16 (3) There might be unresolved differences between the measurement techniques, like due to the different spatial and temporal
17 sampling and resolution.

18 In their discussion of the trend discrepancies between the FPH observations and the merged satellite data set Hegglin et al.
19 (2014) opted for the second possible explanation, indicating that the temporal behaviour at Boulder is different than for the
20 zonal mean of the latitude band around the Boulder latitude. Trends derived from the CMAM simulations at 100 hPa (con-
21 sidering the time period 1980 to 2010) indicated longitudinal differences at 40°N , but also at other latitudes. Subsampling
22 the simulations to Boulder yielded better correlations with the FPH observations, in particular with respect to interannual
23 variations. Yet, the trends derived from the FPH observations and model simulations still disagreed, even in sign.

24 In this study we compare trend estimates for the Boulder location and the zonal mean of the latitude band around the Boulder
25 latitude using several model simulations and observational data sets. This aims to understand how much the sampling bias
26 contributes to the trend discrepancies shown in the lower panel of Fig. 1. The observations are meant to study this aspect on a
27 decadal scale while the simulations will be used to analyse even longer time periods. In the next section the model simulations
28 and observational data sets are briefly described. Section 3 outlines the analysis approach. The results of our analysis are
29 presented in Sect. 4 and subsequently discussed in Sect. 5.

1 2 Data sets

2 In our analysis we primarily utilise model simulations. We consider results from EMAC, WACCM, CMAM and CLaMS. On
3 the observational side we consider data from UARS/HALOE, Envisat/MIPAS and Aura/MLS. These data sets are analysed



4 individually to avoid potential uncertainties and artefacts due to merging (e.g. Ball et al., 2017), providing results for the time
5 periods 1992 – 2005, 2002 – 2012 and 2004 – 2016, respectively.

6 **2.1 Model simulations**

7 **2.1.1 EMAC**

8 The EMAC model is a numerical chemistry and climate simulation system that includes sub-models describing tropospheric
9 and middle atmosphere processes and their interaction with oceans, land and human influences (Jöckel et al., 2010). It uses the
10 second version of the Modular Earth Submodel System (MESSy2) to link multi-institutional computer codes. The core atmo-
11 spheric model is the 5th generation European Centre Hamburg general circulation model (ECHAM5, Roeckner et al., 2006).
12 For the present study we applied EMAC (ECHAM5 version 5.3.02, MESSy version 2.50.5) in the T42L90MA-resolution,
13 i.e. with a spherical truncation of T42 (corresponding to a quadratic Gaussian grid of approximately 2.8° by 2.8° in latitude
14 and longitude) with 90 vertical hybrid pressure levels up to 0.01 hPa. The simulation was set up in accordance to the REF-
15 C1SD (transient hindcast reference simulation with specified dynamics) scenario defined in the framework of the SPARC
16 (Stratosphere-troposphere Processes And their Role in Climate) Chemistry-Climate Model Initiative (Eyring et al., 2013). Cor-
17 respondingly, it considers nudging (by Newtonian relaxation) towards data from the Interim ECMWF (European Centre for
18 Medium-Range Weather Forecasts) Reanalysis project (ERA-interim, Dee et al., 2011). Nudged parameters were the vorticity,
19 divergence, the logarithm of the surface pressure, the temperature and the mean temperature (wave number zero in spectral
20 space, Jöckel et al., 2016). Correspondingly, water vapour itself was not nudged and allowed to evolve freely. Depending on
21 parameter the nudging time constant varied between 6 h and 48 h. The initial conditions (in 1979) were taken from a corre-
22 sponding free-running simulation. In our analysis we use 10 hourly data, lasting until 2013.

23 **2.1.2 WACCM**

24 WACCM is an atmospheric component of the Community Earth System Model (CESM, Hurrell et al., 2013), a global climate
25 model with interactive ocean, sea ice, land and atmosphere. WACCM itself extends from the Earth's surface into the thermo-
26 sphere up to $5.1 \cdot 10^{-6}$ hPa (about 140 km). The simulation used 88 vertical levels and its horizontal resolution amounts to
27 1.9° in latitude and 2.5° in longitude (Marsh et al., 2013). As EMAC, the WACCM simulation employed here was set up ac-
28 cording to the REF-C1SD scenario. Meteorological fields from the MERRA (Modern Era Retrospective-Analysis for Research
29 and Applications, Rienecker et al., 2011) reanalysis data set were nudged from the surface to 50 km. Above 60 km the model
30 meteorological fields were fully interactive, with a linear transition in between. Here, temperature, zonal and meridional winds
31 and surface pressure were used to drive the physical parameterisation that control boundary layer exchanges, advective and
1 convective transport and the hydrological cycle. The nudging time constant used in this study was 50 h. The initial conditions
2 for the year 1979 were taken from a time-dependent REF-C1 simulation that started in 1955. Here we consider daily averaged
3 data and 2014 is the last year of the simulation.



4 2.1.3 CMAM

5 The Canadian Middle Atmosphere Model is a well-established and comprehensive chemistry climate model (de Grandpré
6 et al., 2000; Scinocca et al., 2008). The CMAM simulation we employ is the same that has been used for the merging of the
7 satellite data sets (Hegglin et al., 2014). It covers the period from 1979 to 2010 and provides results from the Earth's surface up
8 to 0.0007 hPa on 63 pressure levels. The horizontal resolution is 3.75° in latitude and longitude (T47). Horizontal winds and
9 temperature data from ERA-interim were nudged up 1 hPa with a nudging time constant of 24 hours at all levels. The nudging
10 was performed in spectral space and only spectral coefficients up to T21 were nudged (McLandress et al., 2013, 2014). For the
11 initial conditions the same simulation setup was run up to 1979, but nudging ERA-40 reanalysis data (Uppala et al., 2005). In
12 our analysis we employ 6 hourly data.

13 2.1.4 CLaMS

14 The CLaMS model is fundamentally different to the models presented so far, as it is a Lagrangian chemistry transport model
15 (McKenna et al., 2002b, a). It is driven by horizontal winds, temperature and diabatic heating rates that are taken from a
16 reanalysis data set. CLaMS uses a hybrid vertical coordinate system which considers isentropes above about 300 hPa. The
17 calculation of water vapour volume mixing ratios is based on simplified dehydration scheme (Ploeger et al., 2013). Below
18 about 500 hPa data from the driving reanalysis are used. Above, if saturation occurs along a trajectory the amount of water
19 vapour in excess of the saturation ratio is frozen out and partly sediments out, based on the fall speed of spherical ice
20 particles of a mean size. Methane oxidation in the stratosphere is implemented using methane fields from the simulation and
21 hydroxyl, oxygen and chlorine radicals from a model climatology. The simulation used in this work was driven by ERA-interim
22 data. The results were interpolated on a regular pressure grid and use a horizontal resolution of 1° in latitude and longitude.
23 We consider daily data (at 12 UTC) until 2010.

24 2.2 Observations

25 2.2.1 UARS/HALOE

26 HALOE was a solar occultation instrument deployed on UARS which was launched on 12 September 1991. Observations lasted
27 until November 2005 shortly before the satellite was decommissioned. Based on the observation geometry 30 observations were
28 performed per day. Those typically covered two distinct latitudes, one in the Northern and one in the Southern Hemisphere.
29 Overall, latitudes between 80°S and 80°N were covered. HALOE measured in the infrared spectral region covering some
30 specific bands between $2.5\ \mu\text{m}$ and $11\ \mu\text{m}$. Water vapour information has been retrieved from a spectral band ranging from $6.54\ \mu\text{m}$
31 μm to $6.67\ \mu\text{m}$, typically covering altitudes from the upper troposphere to the upper mesosphere. In this study we employ data
1 derived with retrieval version 19 (Kley et al., 2000). Occultations with anomalies regarding the trip angle (http://haloe.gats-inc.com/user_docs/events_terminate_below_150km.pdf) and the lockdown angle (http://haloe.gats-inc.com/user_docs/smoothed_



3 lockdown_angles.pdf) were screened out. Also observations before March 1992 were discarded as they might be affected by
4 aerosols from the Pinatubo volcanic eruption in June 1991.

5 **2.2.2 Envisat/MIPAS**

6 MIPAS was a high-resolution Fourier transform spectrometer flown on Envisat. The satellite was launched on 1 March 2002 and
7 operated until 8 April 2012. The MIPAS instrument measured thermal emission in the infrared spectral region between $4.1 \mu\text{m}$
8 and $14.6 \mu\text{m}$ covering the entire latitude range (Fischer et al., 2008). Initially the measurements used a spectral resolution of
9 0.025 cm^{-1} (unapodised). Due to an instrument failure in March 2004 the spectral resolution had to be reduced to 0.0625 cm^{-1} .
10 Observations with the lower spectral resolution recommenced in January 2005. In accordance the MIPAS time period is split in
11 two periods which are referred to as full (FR) and reduced (RR) resolution period. During the FR period more than 1000 scans
12 were performed daily while during the RR period it were more than 1300 scans. Water vapour information is retrieved from
13 12 microwindows between $6.3 \mu\text{m}$ and $12.6 \mu\text{m}$ typically covering the upper troposphere to the middle mesosphere. Here we
14 combine data from the retrieval version 20 for the FR period and version 220/221 for the RR period (Schiederdecker et al.,
15 2015; Lossow et al., 2017), both generated with the research processor operated at IMK/IAA (Institut für Meteorologie und
16 Klimaforschung (IMK) in Karlsruhe, Germany / Instituto de Astrofísica de Andalucía (IAA) in Granada, Spain). The overall
17 time period ranges from July 2002 to April 2012. Before the analysis the data were screened considering the visibility flag
18 and averaging kernel diagonal criterion (discard data with diagonal values < 0.03). The former flags data below the lowermost
19 usable tangent altitude while the latter criterion concerns the measurement contribution to the retrieved data.

20 **2.2.3 Aura/MLS**

21 The Microwave Limb Sounder is an instrument aboard NASA's (National Aeronautics and Space Administration) Aura satel-
22 lite. The satellite was launched on 15 July 2004 and uses a sun-synchronous orbit, as Envisat did. The MLS instrument measures
23 microwave thermal emission at the limb of the Earth's atmosphere, covering the latitude range between 82°S and 82°N . An
24 atmospheric scan takes about 25 s, resulting in more than 3400 observations per day (Waters et al., 2006). Water vapour infor-
25 mation is derived from the strong emission line centred at 183 GHz, covering the altitude range from the upper troposphere
26 to the upper mesosphere. In the analysis we used data from the latest retrieval version 4.2, considering the time period from
27 August 2004 to December 2016. Prior any analysis the data were screened according to the criteria listed in the data quality
28 document (Livesey et al., 2015).

29 **2.2.4 NOAA frost point hygrometer**

30 For the sake of completeness we provide here also a more detailed description of the NOAA frost point hygrometer. The FPH
31 measurement principle is based on maintaining a thin, stable layer of frost on a chilled mirror as air flows past it at $5 \text{ m} \cdot \text{s}^{-1}$.
32 Stability in frost coverage is detected optically and maintained by rapidly adjusting the mirror temperature. When the frost
1 coverage is stable, the ice and overlying water vapour are in equilibrium and the ice surface temperature (frost point tempera-



2 ture) is directly related to the partial pressure of water vapour in the air stream. At 50 hPa, a 0.5 ppmv (about 10%) change in
3 the water vapour mixing ratio produces a 0.42 K change in the frost point temperature. The mirror temperature is measured by
4 a thermistor calibrated to an accuracy better than 0.05 K. Hall et al. (2016) provide detailed descriptions of the instrument and
5 its history, along with an assessment of its measurement uncertainties. The primary measurement uncertainty is related to in-
6 stabilities in frost coverage that can produce frost point temperature errors as large as ± 0.5 K in the stratosphere. However, the
7 instabilities are generally oscillatory in nature and therefore manifest as random errors, not systematic biases. Each thermistor
8 is meticulously calibrated against a temperature probe certified by the National Institute of Standards and Technology (NIST)
9 and, to ensure calibration stability over the long term (i.e. decades), a small archive of previously calibrated thermistors. Total
10 FPH measurement uncertainties (95% confidence) in the stratosphere are estimated to be smaller than 0.3 ppmv (about 6%,
11 Hall et al., 2016). The 30 year net increase (~ 1 ppmv, see Introduction) in stratospheric water vapour observed over Boulder
12 translates to a 0.8 K rise in frost point temperatures that greatly exceeds the FPH measurement uncertainties.

13 3 Approach

14 3.1 Boulder time series

15 For the Boulder time series we consider simulated data and satellite observations that are spatially located within:

- 16 • a 1000 km radius around the Boulder FPH observation site.
- 17 • the latitude band between $35^{\circ}\text{N} - 45^{\circ}\text{N}$.

18 In the analysis of the HALOE data set we use less strict criteria because of its sparseness relative to the other data sets.
19 Instead of the radius criterion data in the wider longitude range between 130°W and 80°W are considered.

20 In temporal terms we consider for the Boulder time series two sets of data. Set #1 simply comprises all data in a given month.
21 We will refer to these time series as full time series. Set #2 is adapted to the individual FPH observations at Boulder. From that
22 we can also assess the role of the temporal component of the sampling bias. For the simulations the data from the closest time
23 step are used. For the observations all data obtained within ± 12 h of the FPH measurements are considered. These time series
24 we will refer to as adapted time series.

25 All data obeying the spatial and temporal criteria are combined to monthly means. For the observations we consider only
26 monthly means that are based on at least 5 measurements to avoid spurious results. As a result, a temporal adaption to the
27 individual FPH observations is only meaningful for the MLS observations.

1 3.2 Zonal mean time series

2 For the zonal mean time series we consider monthly means of all data in the latitude range between 35°N to 45°N , resembling
3 the merged satellite data set. Monthly zonal means derived from the satellite observations are discarded if they are not based
4 on a minimum number of 20 measurements. If a monthly mean does not exist for the Boulder time series, e.g. because there



5 were no FPH observations for the adapted time series or due to screening of the satellite data, this monthly mean is also not
6 considered for the zonal mean results.

7 In addition, we also investigate how the trend estimates at Boulder compare to those for zonal means of other latitude bands.
8 For that we consider the latitude bands 45°N – 55°N, 25°N – 35°N, Equator – 60°N and 60°S – 60°N. The first two bands
9 are adjacent to the latitude band around the Boulder latitude. The last two bands cover a wider range of latitudes. This aims to
10 investigate how representative trends at Boulder are on regional and more global scales.

11 3.3 De-seasonalisation

12 In our analysis we employ de-seasonalised data. This enhances the visibility of the long-term behaviour and has the positive
13 side effect that the MIPAS observations from the FR and RR periods are homogenised. Typically between these periods a small
14 bias in the absolute water vapour volume mixing ratios exists. The de-seasonalisation is achieved by means of regression, again
15 motivated by the MIPAS data. This approach has the advantage of working for time series that cover a time period between
16 12 months and 24 months, which applies here to the MIPAS data for the FR period. The regression model contains an offset
17 and a parametrisation for the semi-annual (SAO) and annual variation (AO) using orthogonal sine and cosine functions:

$$\begin{aligned} f_d(t, \phi, z) = & C_{\text{offset}}(\phi, z) + \\ & C_{\text{SAO}_1}(\phi, z) \cdot \sin(2 \cdot \pi \cdot t / p_{\text{SAO}}) + \\ & C_{\text{SAO}_2}(\phi, z) \cdot \cos(2 \cdot \pi \cdot t / p_{\text{SAO}}) + \\ & C_{\text{AO}_1}(\phi, z) \cdot \sin(2 \cdot \pi \cdot t / p_{\text{AO}}) + \\ & C_{\text{AO}_2}(\phi, z) \cdot \cos(2 \cdot \pi \cdot t / p_{\text{AO}}). \end{aligned} \quad (1)$$

19 In the equation $f_d(t, \phi, z)$ denotes the fit of the regressed time series for a given time t (in years), latitude band ϕ and al-
1 titude z which is subsequently subtracted from the absolute time series to obtain the de-seasonalised time series. C are the
2 regression coefficients of the individual model components and p_{SAO} and p_{AO} represent the time periods of the semi-annual
3 (0.5 years) and annual variation (1 year), respectively. The regression coefficients are derived according to the method outlined
4 by von Clarmann et al. (2010), using the standard errors of the monthly means (their inverse squared) as statistical weights.
5 Autocorrelation effects and empirical errors (Stiller et al., 2012) are not considered in this regression.

6 For the de-seasonalisation of the simulations we consider data in the time period from 1985 to 2010. The start year is
7 chosen because of obvious differences in the water vapour abundances among the simulations, related to differences in their
8 initial conditions and spin up time (see Fig. 2 and Sect. 4.1). 2010 is the last year that is covered by all simulations. For the
9 observations it is not possible to use a consistent time period. Instead the entire time period covered by the individual data sets
10 is used for the de-seasonalisation.



11 3.4 Trend estimates and trend differences

12 Like the de-seasonalisation of the time series, the estimation of the water vapour trends is based on regression. For this analysis
 13 the regression model is as follows:

$$\begin{aligned}
 f_t(t, \phi, z) = & C_{\text{offset}}(\phi, z) + C_{\text{trend}}(\phi, z) \cdot t + \\
 & C_{\text{SAO}_1}(\phi, z) \cdot \sin(2 \cdot \pi \cdot t / p_{\text{SAO}}) + \\
 & C_{\text{SAO}_2}(\phi, z) \cdot \cos(2 \cdot \pi \cdot t / p_{\text{SAO}}) + \\
 & C_{\text{AO}_1}(\phi, z) \cdot \sin(2 \cdot \pi \cdot t / p_{\text{AO}}) + \\
 & C_{\text{AO}_2}(\phi, z) \cdot \cos(2 \cdot \pi \cdot t / p_{\text{AO}}) + \\
 & C_{\text{QBO}_1}(\phi, z) \cdot \text{QBO}_1(t) + \\
 14 & C_{\text{QBO}_2}(\phi, z) \cdot \text{QBO}_2(t).
 \end{aligned} \tag{2}$$

15 In comparison to the regression model used for the de-seasonalisation, it contains in addition a trend term C_{trend} and a
 16 parametrisation for the quasi-biennial oscillation (QBO). In our analysis we determine only a single trend for the entire
 17 time period. Trend changes within this period are correspondingly not analysed (see e.g. Hurst et al., 2011). Even though
 18 the regression is applied to de-seasonalised time series the SAO and AO terms are kept since the regression models for the
 1 de-seasonalisation and trend analysis differ. The QBO parametrisation is based on normalised winds at 50 hPa (QBO_1) and
 2 30 hPa (QBO_2) observed over Singapore (1°N, 104°E), which are almost orthogonal. These data are provided by Freie Uni-
 3 versität Berlin (webpage: <http://www.geo.fu-berlin.de/met/ag/strat/produkte/qbo/qbo.dat>). Unlike for the de-seasonalisation, in
 4 this regression we consider autocorrelation effects and empirical errors (Stiller et al., 2012), to obtain optimal estimates of the
 5 trends and their uncertainties.

6 To be consistent with our motivation shown in Fig. 1, we calculate the water vapour trends separately for the Boulder time
 7 series and the zonal mean time series and subsequently derive the trend differences. Correspondingly, the trend differences
 8 (ΔC_{trend}) and their uncertainties ($\varepsilon_{\text{trend}}$) are given as:

$$\begin{aligned}
 \Delta C_{\text{trend}}(\phi, z) = & C_{\text{trend}}^{\text{Boulder}}(z) - C_{\text{trend}}^{\text{zonal mean}}(\phi, z) \\
 9 \quad \varepsilon_{\text{trend}}(\phi, z) = & \sqrt{\varepsilon_{\text{trend}}^{\text{Boulder}}(z)^2 + \varepsilon_{\text{trend}}^{\text{zonal mean}}(\phi, z)^2}
 \end{aligned} \tag{3}$$

10 Here $C_{\text{trend}}^{\text{Boulder}}$ represents the trends derived from the Boulder time series and $\varepsilon_{\text{trend}}^{\text{Boulder}}$ are the corresponding uncertainties.
 11 Likewise $C_{\text{trend}}^{\text{zonal mean}}$ and $\varepsilon_{\text{trend}}^{\text{zonal mean}}$ denote the trends calculated from the zonal mean time series and their uncertainties.



12 4 Results

13 In this section we will first present the simulation results and subsequently the results derived from the observations. We focus
14 on the altitude range between 100 hPa and 20 hPa that is typically covered by the FPH observations and in almost all cases
15 completely entirely in the stratosphere (Kunz et al., 2013).

16 4.1 Simulations

17 Figure 2 shows for the different model simulations the de-seasonalised Boulder time series (top panel) and the zonal mean
18 time series around the Boulder latitude (latitude range 35°N – 45°N, middle panel) at 70 hPa. The differences between the
19 two time series are shown in the lower panel as a complement. The time series adapted to the individual FPH observations (see
20 Sect. 3.1 and 3.2) are marked with the suffix (A) in the figure legend. Overall, the Boulder and the zonal mean time series are
21 visually rather similar, with the latter being more smooth. The difference time series show occasionally larger deviations (up
22 to 0.6 ppmv in absolute terms), however any conspicuous behaviour or a trend appear to be absent. In general, the different
23 simulations yield similar results for Boulder and the zonal mean. The most prominent exception is observed in the early 1980s.
24 This relates to differences in the 1979 initial conditions and the spin up times among the simulations. Until 1985 the EMAC
25 anomalies are significantly lower than for the other simulations. In the first years the largest anomalies are found in the CMAM
26 results, which were probably caused by higher water vapour volume mixing ratios in the initial conditions based on the nudging
27 of ERA-40 data (see Sect. 2.1.3). Presumably the best representation is provided by CLaMS which, as a Lagrangian model,
28 does not need to deal with these aspects.

29 Figure 3 shows the trend estimates for the time series at Boulder (left column) and the zonal mean for the latitude band
30 between 35°N and 45°N (middle column). The right column shows the corresponding difference according to Eq. 3. The
31 different rows consider different time periods, i.e. 1985 – 2010 (top row), 1990 – 2010 (middle row) and 1995 – 2010 (bottom
32 row), as also indicated in the title of the centre panels. We have not included the time period from 1980 to 2010 here. The
33 differences in the water vapour anomalies among the simulations in the early 1980s primarily affect the trends for Boulder and
1 the zonal mean, yet the trend differences are comparable to those for the time period from 1985 to 2010. Trends and trend
2 differences significant at the 2σ uncertainty levels are marked by triangles.

3 For the time period between 1985 and 2010, the EMAC results exhibit positive trend estimates at Boulder. They range
4 between $0.04 \text{ ppmv} \cdot \text{decade}^{-1}$ and $0.12 \text{ ppmv} \cdot \text{decade}^{-1}$. The trends derived from the adapted time series yield smaller
5 values as those obtained from the full time series, by about $0.02 \text{ ppmv} \cdot \text{decade}^{-1}$ to $0.03 \text{ ppmv} \cdot \text{decade}^{-1}$. The results derived
6 from the other simulations indicate rather small trends at Boulder, typically within $\pm 0.05 \text{ ppmv} \cdot \text{decade}^{-1}$. A few differences
7 exist in the actual sign of the trends, most prominently above 40 hPa where the WACCM and CMAM results indicate negative
8 trends (around $-0.04 \text{ ppmv} \cdot \text{decade}^{-1}$) while they are positive for CLaMS (up to around $0.05 \text{ ppmv} \cdot \text{decade}^{-1}$ at 20 hPa).
9 The results derived from the full and the adapted time series exhibit small quantitative differences. Typically they are of a
10 similar size as those described above for the EMAC results. Overall, the spread among the trend estimates ranges from about
11 $0.10 \text{ ppmv} \cdot \text{decade}^{-1}$ at 100 hPa to $0.16 \text{ ppmv} \cdot \text{decade}^{-1}$ at 20 hPa. The trend estimates derived from the zonal mean time



12 series for the latitude band between 35°N and 45°N look very similar to those derived for Boulder. Correspondingly, the
13 trend differences between Boulder and the zonal mean are very small. The differences never exceed $0.04 \text{ ppmv} \cdot \text{decade}^{-1}$ in
14 absolute terms. The largest differences are derived for EMAC and WACCM (based on the adapted time series) at 100 hPa. The
15 trend differences are predominantly positive below 70 hPa and mostly negative above 50 hPa. The exact altitude dependence
16 differs in details among the different simulation results.

17 Both for Boulder and the zonal mean, the trend estimates for the time period from 1990 to 2010 are negative. There
18 are differences among the individual simulations. The agreement is, however, better than for the time period between 1985
19 and 2010. The spread maximises at 100 hPa with about $0.12 \text{ ppmv} \cdot \text{decade}^{-1}$ and is smallest above 40 hPa with about
20 $0.06 \text{ ppmv} \cdot \text{decade}^{-1}$. Differences among the results derived from the full and adapted time series are very small. The trend
21 differences between Boulder and the zonal mean are of similar size as for the time period 1985 to 2010. A similar behaviour
22 in terms of the altitude dependence is also visible.

23 The last time period we consider is from 1995 to 2010. At 100 hPa consistently positive trends are found, except for the
24 adapted EMAC time series. Overall, the trend estimates vary between $-0.02 \text{ ppmv} \cdot \text{decade}^{-1}$ and $0.14 \text{ ppmv} \cdot \text{decade}^{-1}$.
25 With increasing altitude the trend estimates typically decrease and above 45 hPa they are all negative. The decrease continues
26 up to 20 hPa, except for the CMAM results which indicate a slight increase above 40 hPa. At 20 hPa the trend estimates vary
27 between $-0.24 \text{ ppmv} \cdot \text{decade}^{-1}$ and $-0.08 \text{ ppmv} \cdot \text{decade}^{-1}$ among the simulations, with significantly smaller differences
28 between the results derived from the full and the adapted time series. The best agreement among the simulations is observed
29 around 80 hPa where the spread is about $0.08 \text{ ppmv} \cdot \text{decade}^{-1}$. The altitude dependence and the spread among the simulations
30 is similar for the trend estimates derived from the zonal mean time series. Quantitatively there are larger differences between
31 the Boulder and zonal mean trends, clearly surpassing those observed for the other time periods. Above 60 hPa the differences
32 are still within $\pm 0.02 \text{ ppmv} \cdot \text{decade}^{-1}$. Below this altitude the differences occasionally exceed $\pm 0.05 \text{ ppmv} \cdot \text{decade}^{-1}$. The
33 largest trend differences are derived from the adapted EMAC and CMAM time series.

34 To expand on the temporal development of the trend differences between Boulder and the zonal mean even more we derive
35 these differences continuously for 11 year periods, as shown in Fig. 4. This aims also to build a bridge to the shorter observa-
1 tional results that will be presented in Sect. 4.2. The results are assigned to the centre of the considered period, e.g. to 1995
2 for the time period between 1990 and 2000. The trend differences vary with time and altitude in size and sign. On this shorter
3 time scale the differences are typically larger than observed for the longer time periods described in the last figure. There is
4 also a more prominent distinction between the results derived from the full and the adapted time series. The latter yield larger
5 differences on an absolute scale, but also some patterns are different.

6 For the full time series the trend differences are generally within $\pm 0.04 \text{ ppmv} \cdot \text{decade}^{-1}$. Exceptions from this behaviour are
7 primarily observed at the lowermost altitudes. In particular the EMAC results exhibit significantly larger differences, increasing
8 to about $\pm 0.15 \text{ ppmv} \cdot \text{decade}^{-1}$ at 100 hPa. The temporal development of the trend differences exhibits a number of common
9 features among the simulations, even though quantitative differences are obvious. At the lowermost altitudes all simulations
10 show negative trend differences from 1990 to about 1999. Afterwards positive trend differences are found. Higher up, i.e. above
11 about 50 hPa, positive trend differences are visible from 1995 to about 2004.



12 The trend differences derived from the adapted time series are within ± 0.08 ppmv · decade⁻¹ above 60 hPa. Below, they
13 increase again to about 0.2 ppmv · decade⁻¹ in absolute terms. The different simulations agree on some difference patterns, as
14 observed for the results derived from the full time series. Most prominently, above 50 hPa the trend differences are typically
15 positive from about 1990 to 2003 and negative afterwards. The bisection of trend differences at the lowermost altitudes derived
16 from the full time series is only visible in some simulations. Finally, it should be noted, that none of the trend differences shown
17 in Fig. 4 are statistically significant at the 2σ uncertainty level.

18 To investigate the representativeness of the Boulder trends on a larger geographical scale Fig. 5 compares them to the trends
19 derived from zonal mean time series from five latitude bands, namely 35°N – 45°N (row #1), 45°N – 55°N (row #2), 25°N –
20 35°N (row #3), Equator – 60°N (row #4) and 60°S – 60°N (row #5). The figure considers the time period between 1987
21 and 2010, approximately the time coverage of the merged zonal mean satellite data set. The results in the left column are the
22 same for all rows and kept for the sake of convenience. The trends at Boulder are close to those obtained for the time periods
23 1985 – 2010 and 1990 – 2010 shown in Fig. 3. Note, that in Fig. 5 the x-axis is smaller, allowing a more detailed picture.

24 Overall, the trends at Boulder are within ± 0.07 ppmv · decade⁻¹. Clear differences among the simulations exist, while the
25 differences between the results derived from the full and the adapted time series are typically smaller. The EMAC results
26 indicate positive trends (up to almost 0.1 ppmv · decade⁻¹). Statistical significance is only visible at the highest altitudes.
27 The trend estimates derived from the adapted time series are again smaller than those determined from the full time series.
28 With few exceptions the same behaviour is also observed for all other simulations. The trends derived from CLaMS are
29 negative below 35 hPa and positive above, ranging from about -0.05 ppmv · decade⁻¹ to 0.05 ppmv · decade⁻¹. They are
30 relatively constant up to 60 hPa before they start to increase significantly. The WACCM and CMAM trends show a similar
31 altitude dependence with maximum negative trends (around -0.05 ppmv · decade⁻¹) in the altitude range between 50 hPa
32 and 40 hPa. For WACCM the trend estimates become positive below 80 hPa while those derived from the CMAM simulations
33 are negative at all altitudes.

34 As observed in Fig. 3 the trends derived from the zonal mean time series for the latitude band between 35°N and 45°N are
35 very similar to those for Boulder. Correspondingly, the trend differences are small, i.e. ranging from -0.02 ppmv · decade⁻¹
1 to 0.04 ppmv · decade⁻¹. The differences are typically positive below 70 hPa and mostly negative above, affirming the picture
2 observed for the time periods 1985 – 2010 and 1990 – 2010 in Fig. 3.

3 The trends derived from the zonal mean time series for the other latitude bands exhibit many common features with the
4 results for the zonal mean between 35°N and 45°N. There are quantitative changes, but overall the trend estimates remain of
5 the same order. Besides that, also the altitude dependence of the trends remains very similar and so do the relations among
6 the different simulations. The trend differences between Boulder and the zonal mean for 45°N and 55°N remain within
7 ± 0.04 ppmv · decade⁻¹. Again, the differences are typically positive below 70 hPa and predominantly negative at higher
8 altitudes. The trend differences between Boulder and the zonal means for 25°N to 35°N and from the Equator to 60°N are
9 quite similar, at least up to about 35 hPa. In both cases the trend differences are within ± 0.03 ppmv · decade⁻¹. Typically
10 the EMAC and CLaMS results are at the higher end of this interval while the WACCM and CMAM results are at the lower
11 end. The largest trend differences compared to Boulder are observed for the zonal mean of the latitude band between 60°S



12 and 60°N. These range from $-0.04 \text{ ppmv} \cdot \text{decade}^{-1}$ to slightly more than $0.06 \text{ ppmv} \cdot \text{decade}^{-1}$. There is clear separation
13 between the CLaMS results and those from the other simulations. For the CLaMS simulation the trend differences are negative
14 at 100 hPa (around $-0.015 \text{ ppmv} \cdot \text{decade}^{-1}$). Around 90 hPa they turn positive and continue to increase within increasing
15 altitude. At 20 hPa the differences amount to $0.05 \text{ ppmv} \cdot \text{decade}^{-1}$ for the adapted time series and $0.06 \text{ ppmv} \cdot \text{decade}^{-1}$
16 for the full time series, respectively. The other simulations indicate positive trend differences at 100 hPa. Around 70 hPa the
17 differences become negative and peak in absolute size between 50 hPa and 40 hPa (between $-0.04 \text{ ppmv} \cdot \text{decade}^{-1}$ and
18 $-0.02 \text{ ppmv} \cdot \text{decade}^{-1}$). Higher up, the trend differences get less negative again.

19 4.2 Observations

20 Figure 6 shows for the HALOE, MIPAS and MLS observations the de-seasonalised Boulder time series (top panel) and the
21 zonal mean time series around the Boulder latitude at 70 hPa (middle panel). As in Fig. 2 the lower panel shows the differences
22 between the two time series in addition. For MLS there is also a data set that is adapted to the FPH observations at Boulder (see
23 Sect 3.1). Like the simulations the observations exhibit a rather similar picture for Boulder and the zonal mean. The difference
24 time series indicate occasionally some larger deviations. For example in the second half of 2011 some substantial positive
25 differences are observed, consistent in the MIPAS and MLS data. The largest differences typically occur in the MLS data set
26 that is adapted to the FPH observations and for HALOE data set, primarily due to its sparseness. In addition, there is a notable
27 agreement between the MIPAS and MLS time series for Boulder and the zonal mean time series.

28 Figure 7 compares the trend estimates at Boulder with those derived from zonal mean time series for various latitude bands.
29 The results for the different observational data sets consider different time periods as indicated in the figure legend. Thus, they
30 are not comparable and will be addressed separately.

31 In the lower stratosphere the HALOE observations exhibit negative trends at Boulder for the time period between 1992
32 and 2005. This behaviour is primarily related to the significant drop in lower stratospheric water vapour in 2001 (Randel
33 et al., 2006; Scherer et al., 2008; Brinkop et al., 2016). The relative dryness continued until 2005 (coinciding with the end of
34 the HALOE observations), causing the 13 year HALOE trends to be negative. The largest trends are observed below 80 hPa
1 with values around $-0.45 \text{ ppmv} \cdot \text{decade}^{-1}$. Above, the trends get less negative with increasing altitude. At 20 hPa the trend
2 amounts to about $-0.03 \text{ ppmv} \cdot \text{decade}^{-1}$ (and is not statistically significant). The trends derived for the zonal mean between
3 35°N to 45°N have a similar altitude dependence, but their absolute sizes are smaller. Accordingly, the trend differences
4 between Boulder and the zonal mean are negative. Above 80 hPa the differences are almost invariant with altitude. Here they
5 amount to about $-0.05 \text{ ppmv} \cdot \text{decade}^{-1}$. At lower altitudes the differences are larger maximising at 100 hPa with about
6 $-0.1 \text{ ppmv} \cdot \text{decade}^{-1}$. For the other latitude bands the zonal mean trends exhibit the same kind of altitude dependence as
7 observed for the band from 35°N to 45°N. The most prominent variation concerns the exact altitude in which the negative
8 trends exhibit their absolute maximum. For the latitude band between 45°N and 55°N this occurs close to 90 hPa. For the
9 trends derived from the zonal mean from the Equator to 60°N and from 60°S to 60°N this maximum is observed around
10 70 hPa. The trend differences between Boulder and the zonal mean for the latitude band between 45°N and 55°N range from
11 $-0.1 \text{ ppmv} \cdot \text{decade}^{-1}$ to $0 \text{ ppmv} \cdot \text{decade}^{-1}$ with the largest absolute values occurring below 75 hPa. For the latitude band



12 between 25°N and 35°N the trend differences are close to zero, except below 75 hPa where they become significantly more
13 negative. For the remaining two latitude bands the trend differences are quite similar. At 100 hPa the trend differences amount
14 to $-0.15 \text{ ppmv} \cdot \text{decade}^{-1}$. Towards 60 hPa the differences increase to around $0.05 \text{ ppmv} \cdot \text{decade}^{-1}$. Between 60 hPa and
15 30 hPa the trend differences are rather constant. Higher up, they increase to more than $0.1 \text{ ppmv} \cdot \text{decade}^{-1}$.

16 The MIPAS observations indicate positive trends at Boulder during the time period from 2002 to 2012. The trends decrease
17 with increasing altitude from about $0.25 \text{ ppmv} \cdot \text{decade}^{-1}$ at 100 hPa to $0.1 \text{ ppmv} \cdot \text{decade}^{-1}$ at 20 hPa. For the zonal mean
18 between 35°N and 45°N the trend estimates are also consistently positive. However, they show a slightly different altitude
19 dependence than for Boulder. Below about 70 hPa the trends increase while higher up they decrease. In correspondence,
20 the trend differences between the Boulder and zonal mean estimates are most pronounced below about 70 hPa, rising to
21 $0.05 \text{ ppmv} \cdot \text{decade}^{-1}$ at 100 hPa. Above 70 hPa the differences are close to zero. A very similar behaviour is observed for
22 the trend differences between Boulder and the zonal mean considering the latitude band between 45°N and 55°N. The trend
23 differences to the estimates for the latitude bands from 25°N to 35°N and the Equator to 60°N exhibit a pronounced altitude
24 dependence. They decrease from more than $0.1 \text{ ppmv} \cdot \text{decade}^{-1}$ at 100 hPa to $-0.05 \text{ ppmv} \cdot \text{decade}^{-1}$ at 20 hPa. The sign
25 of the trend differences switches at about 60 hPa. The trend differences between Boulder and the zonal mean for 60°S to 60°N
26 are positive at all altitudes. The smallest differences are close to zero and are observed between 45 hPa and 30 hPa. The largest
27 difference is visible at 100 hPa with $0.15 \text{ ppmv} \cdot \text{decade}^{-1}$.

28 The Boulder trends derived from the MLS observations from 2004 to 2016 are positive. They exhibit a pronounced altitude
29 dependence. The trend estimates exhibit maxima at 70 hPa ($0.4 \text{ ppmv} \cdot \text{decade}^{-1}$) and 30 hPa (close to $0.3 \text{ ppmv} \cdot \text{decade}^{-1}$).
30 Minima are found at 100 hPa ($0.2 \text{ ppmv} \cdot \text{decade}^{-1}$), 45 hPa and 20 hPa (around $0.25 \text{ ppmv} \cdot \text{decade}^{-1}$). The trends derived
31 from the adapted time series are slightly larger than those calculated from the full time series. The trend differences between
32 these two data sets are of a similar order as observed for the simulations addressed before. The MLS trends derived from
33 the zonal mean time series for the different latitudes indicate a similar altitude dependence as that observed for Boulder.

1 Overall, the trend differences between Boulder and the zonal means are generally within $\pm 0.05 \text{ ppmv} \cdot \text{decade}^{-1}$. Prominent
2 exceptions occur below 70 hPa for the differences to the zonal means from 25°N to 35°N, Equator to 60°N and 60°S to 60°N.
3 Here, the differences can be as large as $0.15 \text{ ppmv} \cdot \text{decade}^{-1}$. In addition, the trend differences between Boulder and the
4 zonal mean from 60°S to 60°N are noticeably larger than for the other latitude bands, ranging from $0.05 \text{ ppmv} \cdot \text{decade}^{-1}$
5 to $0.15 \text{ ppmv} \cdot \text{decade}^{-1}$. Beyond that, the trend differences are consistently larger (by about $0.05 \text{ ppmv} \cdot \text{decade}^{-1}$) for the
6 adapted time series at altitudes around 40 hPa.

7 5 Discussion and conclusions

8 In this work we compared trend estimates for lower stratospheric water vapour between Boulder and zonal mean data around
9 the Boulder latitude (35°N to 45°N), considering different simulations and observations. The primary objective was to verify
10 if sampling biases could possibly help to explain the discrepancies in the trend estimates between the FPH observations at
11 Boulder (Hurst et al., 2011) and a merged zonal mean satellite data set (Hegglin et al., 2014). For the time period from the late



12 1980s to 2010 the trend differences (FPH minus merged zonal mean satellite data set) range from $0.25 \text{ ppmv} \cdot \text{decade}^{-1}$ to
13 $0.45 \text{ ppmv} \cdot \text{decade}^{-1}$, increasing with altitude.

14 Our analysis shows that there are differences in the trend estimates between Boulder and the zonal mean, both for the
15 simulations and observations. These trend differences are dependent on altitude and the time period considered. For the
16 time period from the late 1980s to 2010 the simulations indicate trend differences between about $-0.02 \text{ ppmv} \cdot \text{decade}^{-1}$
17 to $0.04 \text{ ppmv} \cdot \text{decade}^{-1}$ (which are however not statistically significant different from zero). These are clearly smaller than
18 the discrepancies in the trend estimates derived from the FPH observations and the merged satellite data set. The larger positive
19 differences are observed close to 100 hPa. Here, the sampling bias partly resolves the observational discrepancies. Above about
20 60 hPa the trend differences derived from the model simulations are however typically negative. This indicates that the trend
21 estimates for the zonal mean data should be larger than at Boulder, which is contradictory to the observed trend differences
22 between the FPH observations and the merged zonal mean satellite data set. For the time period from the late 1980s to 2010,
23 the simulations also do not indicate any significant deviations in the trend differences derived from time series using all data
24 during a given month (which we referred to as full time series) or just using that closest in time to the actual FPH observations
25 (which we referred to as adapted time series). This indicates that the temporal contribution to the sampling bias on this time
26 scale is small.

27 Given these model results, a sampling bias is not a viable explanation for the trend discrepancies between the FPH obser-
28 vations at Boulder and the merged zonal mean satellite data set presented in Hegglin et al. (2014). It still could be the case
29 that the simulations underrepresent variability or that the trend differences originate from smaller spatial and temporal scales
30 than are resolved by the model simulations (i.e. sub-grid processes). For the Boulder time series we used data in a 1000 km
31 radius around the Boulder FPH observation site and within the latitude range from 35°N to 45°N . These criteria were primarily
32 chosen for consistency with the analysis of the satellite observations whose exact measurement locations vary from orbit to
33 orbit and day to day. In an additional analysis of the simulations, we considered for the Boulder time series only data from the
34 closest grid point in space (EMAC: 40.5°N , 104.1°W , $\Delta r=109 \text{ km}$; WACCM: 40.7°N , 105.0°W , $\Delta r=80 \text{ km}$; CMAM: 39.0°N ,
1 105.0°W , $\Delta r=113 \text{ km}$; CLaMS: 40.0°N , 105.0°W , $\Delta r=17 \text{ km}$). This analysis yields small quantitative changes (not shown).
2 Qualitatively, exactly the same conclusions can be drawn as from the standard analysis. The temporal resolutions of the anal-
3 ysed simulations vary (see Sect. 2.1). The CMAM simulations provide the best resolution in this analysis with 6 h. Accordingly
4 the worst temporal mismatch to the actual FPH observations is 3 h. This gives an upper limit of temporal scales not covered
5 in this analysis. Yet, arguably the different simulations yield similar results, as do the analysis of the full and the adapted time
6 series.

7 For a single decade of data the trend differences between Boulder and the $35^{\circ}\text{N} - 45^{\circ}\text{N}$ zonal mean are typically larger
8 than those discussed above for the entire time period from the late 1980s to 2010. The differences are typically within
9 $\pm 0.10 \text{ ppmv} \cdot \text{decade}^{-1}$, except close to 100 hPa where the differences can be occasionally as large as $\pm 0.2 \text{ ppmv} \cdot \text{decade}^{-1}$.
10 For the simulations, the trend differences derived from the adapted time series are typically larger than the trend differences
11 obtained from the full time series on an absolute scale. A factor 2 is a common feature. In the MLS data, significant trend



12 differences between the full and the adapted time series are observed around 40 hPa. These differences should to be kept in
13 mind when comparing results for Boulder and the zonal mean on the shorter time scales.

14 In addition, we analysed trend differences between Boulder and the zonal means for a number of latitude bands. This aimed
15 to investigate how representative the Boulder trends are for a more global scale. For the time period from 1987 to 2010 the
16 simulations indicate trend differences within the interval from $-0.04 \text{ ppmv} \cdot \text{decade}^{-1}$ to $0.06 \text{ ppmv} \cdot \text{decade}^{-1}$. The largest
17 differences occur when the Boulder trends are compared to those for the zonal mean of the latitude band between 60°S and
18 60°N . Based on these results, the Boulder trends should be quite representative (or a reasonable first guess) for the trends on
19 more global scales during this time period. The caveats regarding missing variability or sub-grid processes in the simulations
20 apply here as well. For shorter time periods, as covered by the individual satellite data sets, the representativeness gets smaller
21 in general.

22 From our analysis it appears that a continued search for the reasons of the trend discrepancies between the FPH observations
23 at Boulder and the merged satellite set is necessary (see list in the Introduction). In addition, even more differences become
24 apparent. To start with, this considers the simulations themselves. The overall spread among the trend estimates derived from
25 the different simulations is typically between $0.1 \text{ ppmv} \cdot \text{decade}^{-1}$ and $0.2 \text{ ppmv} \cdot \text{decade}^{-1}$. This certainly sheds a different
26 light on the trend discrepancies between the FPH observations and the merged zonal mean satellite data set, if the spread
27 among different simulations amounts to a significant part of the discrepancies themselves. The reasons for the spread among
28 the simulations are probably manifold, comprising general model characteristics, the choice of the nudged reanalysis data
29 (and their quality over time, Fujiwara et al., 2017) or the exact details of the nudging (see Sect. 2.1). Our analysis does not
30 provide clear hints in a specific direction but leaves room for obvious followup activities. Then, the trend estimates obtained
31 from the simulations also differ from those derived from the FPH observations and the merged satellite data set (compare
32 Fig. 1 and Fig. 5). Overall, they are closer to the trend estimates from the merged satellite data set, but consistently larger
33 by about $0.02 \text{ ppmv} \cdot \text{decade}^{-1}$ to $0.15 \text{ ppmv} \cdot \text{decade}^{-1}$ depending on simulation and altitude. Compared to the FPH trend
34 estimates the model results are consistently smaller by about $0.1 \text{ ppmv} \cdot \text{decade}^{-1}$ to $0.45 \text{ ppmv} \cdot \text{decade}^{-1}$. In many ways
1 this situation is reminiscent to the results presented by Garcia et al. (2007) that indicated clear trend differences between the
2 FPH observations, HALOE and an older version of WACCM for the time period between 1992 and 2002.

3 A way forward is certainly to go away from derived quantities and to look at difference time series of the water vapour
4 anomalies instead. An example of this is shown in Fig. 8 which considers the difference between the de-seasonalised time
5 series derived from the FPH observations at Boulder and the Boulder time series from the different simulations and satellite
6 observations (i.e. FPH minus the other data sets) used in this work at 70 hPa. For the simulations and the MLS data set the
7 adapted Boulder time series are used while for the HALOE and MIPAS data sets the full time series are employed, as also
8 indicated in the legend of the figure. For the de-seasonalisation of the FPH time series the same time period is used as for
9 the model simulations, i.e. from 1985 to 2010 (see Sect. 3.3). For a clearer picture the differences are smoothed with a 1 year
10 running mean. At least three valid data points during this period are required for a running mean to be considered further. The
11 differences visible in the figure are also representative for other altitudes, even though some details are different. Those are



12 also characteristic for differences between FPH time series and the zonal mean time series for the latitude band between 35°N
13 and 45°N. A number of aspects gain attention:

14 (1) Before 1986 the differences to FPH observations are predominantly negative (EMAC being the exception), while after-
15 wards until 2011 they are mostly positive. As the trends in this work are derived by multi-linear regression with a single
16 trend term, this behaviour is consistent with larger trend estimates for the FPH observations compared to the simulations
17 for the time period from the late 1980s to 2010.

18 (2) In addition, we have in the figure included results derived from observations by the SAGE II (Stratospheric Aerosol and Gas
19 Experiment II) instrument aboard ERBS (Earth Radiation Budget Satellite), based on the retrieval version 7.00 (Damadeo
20 et al., 2013). These data are also considered in the merged satellite data set and actually define the start of the time series
21 (Hegglin et al., 2014). The results here consider the zonal mean time series for the latitude band between 35°N and 45°N (as
22 noted in the legend). While the SAGE II differences to the FPH observations mostly blend with the other data sets there is
23 pronounced deviation between 1989 and 1991 (afterwards data are screened due to aerosol contamination by the Pinatubo
24 eruption). During this time period the differences are more negative than for the model simulations. This behaviour is
25 consistently observed below 30 hPa. Since this is close to the very beginning of the merged time series it has a pronounced
26 effect on the trend estimates. It provides an explanation why the trend estimates derived from the merged satellite data set
27 are smaller than those for the simulations considering the time period from the late 1980s to 2010. Overall, this might hint
28 to a potential issue with the SAGE II data before the Pinatubo eruption. Alternatively, an issue might originate from the
29 equal weighting of the pre- and post-Pinatubo data in the merged satellite data set. More investigations are required to rule
30 out any potential issue.

31 (3) The temporal development of the differences is quite consistent in qualitative terms for the various simulations and obser-
32 vational data sets. Features like the strong negative differences around 1993/1994, the subsequent increase until 2000, the
33 relatively constant behaviour from 2001 to 2009 or the decrease starting in 2010 are visible for all simulations and satel-
34 lite observations. Interestingly, we find a similar behaviour also in difference time series between frost point hygrometer
1 observations at other stations and the simulations and satellite observations used in this work (not shown). Explicitly, this
2 applies to the NOAA FPH observations at Lauder (45°S, 169.7°E) and the CFH (cryogenic frost point hygrometer, Vömel
3 et al., 2007) observations at San Jose (9.9°N, 84.0°W) and Lindenberg, (52.2°N, 14.1°E). In quantitative terms, the consis-
4 tency of the differences is evidently is less good. The spread among the various data sets is on average 0.25 ppmv and is,
5 thus, comparable to the differences between the FPH observations and the different simulations and satellite observations
6 themselves. In particular, between 1980 and 1985 there are huge deviations among the simulations in their differences to
7 the FPH observations, relating to differences in the initial conditions and the spin up times among the simulations (except
8 for CLaMS). After this period the average spread decreases to 0.20 ppmv. One caveat is that the time periods for the
9 de-seasonalisation inevitably vary among the satellite data sets and are different from that used for the FPH observations
10 (and model simulations). While this affects the absolute differences, tests show that this has no decisive influence on the
11 overall spread estimate nor the consistency of the temporal development of the differences shown in Fig. 8.



12 In summary, understanding the differences shown in Fig. 8 and their temporal development, hopefully in combination with the
13 merged satellite data set, should be a focal point of further research on lower stratospheric water vapour. This will inevitably
14 yield better consistency in the trend estimates but also highlight the benefit of combining different data sources, as in situ
15 observations, satellite measurements and modelling efforts.

16 *Data availability.*

17

18 Simulations:

19 – The data of the EMAC simulation described above will be made available in the Climate and Environmental Retrieval and Archive
20 (CERA) database at the German Climate Computing Centre (DKRZ, website: <http://cera-www.dkrz.de/WDCC/ui/Index.jsp>). The cor-
21 responding digital object identifiers (DOI) will be published on the MESSy consortium website (<http://www.messy-interface.org>).
22 Alternatively, the data can be obtained on request from Patrick Jöckel (patrick.joeckel@dlr.de).

23 – The WACCM data can be obtained on request from Doug Kinnison (dkin@ucar.edu).

24 – The CMAM simulation can be accessed from the following webpage: <http://www.ccmma.ec.gc.ca/data/cmam/CMAM/index.shtml>.

25 – The CLaMS data can be obtained on request from Felix Ploeger (f.ploeger@fz-juelich.de).

26 Observations:

27 – The NOAA FPH data observed at Boulder can be downloaded from the FTP address [ftp://ftp.cmdl.noaa.gov/data/ozwv/WaterVapor/
28 Boulder_LEV](ftp://ftp.cmdl.noaa.gov/data/ozwv/WaterVapor/Boulder_LEV) or alternatively obtained on request from Dale Hurst (dale.hurst@noaa.gov).

29 – The HALOE data can be accessed on the following website: <http://haloe.gats-inc.com/download/index.php>.

1 – The MIPAS data are available on the following website: <https://www.imk-asf.kit.edu/english/308.php>.

2 – The MLS data can be downloaded from the following website: [https://acdisc.gesdisc.eosdis.nasa.gov/data/Aura_MLS_Level2/ML2H2O.
3 004/](https://acdisc.gesdisc.eosdis.nasa.gov/data/Aura_MLS_Level2/ML2H2O.004/).

4 – The SAGE II data can be accessed from the following website: https://eosweb.larc.nasa.gov/project/sage2/sage2_table.

5 *Competing interests.* The authors declare that they have no conflict of interest.

6 *Acknowledgements.* S. Lossow was funded by the DFG Research Unit “Stratospheric Change and its Role for Climate Prediction” (SHARP)
7 under contract STI 210/9-2. The UTLS water vapour measurement record at Boulder, comprised of monthly balloon flights of the NOAA
1 FPH, continues in its 38th year thanks to funding from the NOAA Climate Program Office, the NASA Earth Science Division’s Upper
2 Atmospheric Composition Observations programme and the US Global Climate Observing System programme. We appreciate the HALOE
3 Science Team and the many members of the HALOE project for producing and characterising the high quality HALOE data set. We would
4 like to thank the European Space Agency (ESA) for making the MIPAS level-1b data set available. MLS data were obtained from the NASA



- 5 Goddard Earth Sciences and Information Center. Work at the Jet Propulsion Laboratory, California Institute of Technology, was done under
6 contract with the National Aeronautics and Space Administration. The EMAC simulations have been performed at the German Climate
7 Computing Centre (DKRZ) through support from the Bundesministerium für Bildung und Forschung (BMBF). DKRZ and its scientific
8 steering committee are gratefully acknowledged for providing the high performance computing (HPC) and data archiving resources for
9 ESCiMo (Earth System Chemistry integrated Modelling) consortial project. We thank Ted Shepherd for valuable comments on an early
10 version of this manuscript.
- 11 We acknowledge support by Deutsche Forschungsgemeinschaft and Open Access Publishing Fund of Karlsruhe Institute of Technology.



12 References

- 13 Avery, M. A., Davis, S. M., Rosenlof, K. H., Ye, H., and Dessler, A. E.: Large anomalies in lower stratospheric water vapour and ice during
14 the 2015-2016 El Niño, *Nature Geoscience*, 10, 405 – 409, <https://doi.org/10.1038/ngeo2961>, 2017.
- 15 Ball, W. T., Alsing, J., Mortlock, D. J., Rozanov, E. V., Tummon, F., and Haigh, J. D.: Reconciling differences in stratospheric ozone
16 composites, *Atmospheric Chemistry & Physics*, 17, 12 269 – 12 302, <https://doi.org/10.5194/acp-17-12269-2017>, 2017.
- 17 Brasseur, G. and Solomon, S.: *Aeronomy of the middle atmosphere*, Springer, ISBN-10 1-4020-3284-6, P.O. Box 17, 3300 AA Dordrecht,
18 The Netherlands, 2005.
- 19 Brinkop, S., Dameris, M., Jöckel, P., Garny, H., Lossow, S., and Stiller, G.: The millennium water vapour drop in chemistry-climate model
20 simulations, *Atmospheric Chemistry & Physics*, 16, 8125 – 8140, <https://doi.org/10.5194/acp-16-8125-2016>, 2016.
- 21 Damadeo, R. P., Zawodny, J. M., Thomason, L. W., and Iyer, N.: SAGE version 7.0 algorithm: application to SAGE II, *Atmospheric
22 Measurement Techniques*, 6, 3539 – 3561, <https://doi.org/10.5194/amt-6-3539-2013>, 2013.
- 23 de Grandpré, J., Beagley, S. R., Fomichev, V. I., Griffioen, E., McConnell, J. C., Medvedev, A. S., and Shepherd, T. G.: Ozone climatology
24 using interactive chemistry: Results from the Canadian Middle Atmosphere Model, *Journal of Geophysical Research*, 105, 26 475 –
25 26 492, <https://doi.org/10.1029/2000JD900427>, 2000.
- 26 Dee, D. P., Uppala, S. M., Simmons, A. J., Berrisford, P., Poli, P., Kobayashi, S., Andrae, U., Balmaseda, M. A., Balsamo, G., Bauer,
27 P., Bechtold, P., Beljaars, A. C. M., van de Berg, L., Bidlot, J., Bormann, N., Delsol, C., Dragani, R., Fuentes, M., Geer, A. J., Haim-
28 berger, L., Healy, S. B., Hersbach, H., Hólm, E. V., Isaksen, I., Kållberg, P., Köhler, M., Matricardi, M., McNally, A. P., Monge-Sanz,
29 B. M., Morcrette, J.-J., Park, B.-K., Peubey, C., de Rosnay, P., Tavolato, C., Thépaut, J.-N., and Vitart, F.: The ERA-Interim reanalysis:
30 configuration and performance of the data assimilation system, *Quarterly Journal of the Royal Meteorological Society*, 137, 553 – 597,
31 <https://doi.org/10.1002/qj.828>, 2011.
- 32 Dessler, A. E., Schoeberl, M. R., Wang, T., Davis, S. M., and Rosenlof, K. H.: Stratospheric water vapor feedback, *Proceedings of the
33 National Academy of Science*, 110, 18 087 – 18 091, <https://doi.org/10.1073/pnas.1310344110>, 2013.
- 34 Dessler, A. E., Ye, H., Wang, T., Schoeberl, M. R., Oman, L. D., Douglass, A. R., Butler, A. H., Rosenlof, K. H., Davis, S. M., and Portmann,
35 R. W.: Transport of ice into the stratosphere and the humidification of the stratosphere over the 21st century, *Geophysical Research Letters*,
36 43, 2323 – 2329, <https://doi.org/10.1002/2016GL067991>, 2016.
- 1 Dvortsov, V. L. and Solomon, S.: Response of the stratospheric temperatures and ozone to past and future increases in stratospheric humidity,
2 *Journal of Geophysical Research*, 106, 7505 – 7514, <https://doi.org/10.1029/2000JD900637>, 2001.
- 3 Eyring, V., Lamarque, J.-F., Hess, P., Arfeuille, F., Bowman, K., Chipperfield, M. P., Duncan, B., Fiore, A., Gettelman, A., Giorgetta,
4 M. A., Granier, C., Hegglin, M. I., Kinnison, D., Kunze, M., Langematz, U., Luo, B., Martin, R., Matthes, K., Newman, P. A., Peter, T.,
5 Robock, A., Ryerson, T., Saiz-Lopez, A., Salawitch, R., Schultz, M., Shepherd, T. G., Shindell, D., Staehelin, J., Tegtmeier, S., Thomason,
6 L., Tilmes, S., Vernier, J.-P., Waugh, D. W., and Young, P. J.: Overview of IGAC/SPARC Chemistry-Climate Model Initiative (CCMI)
7 community simulations in support of upcoming ozone and climate assessments, *SPARC Newsletter*, 40, 48 – 66, 2013.
- 8 Fischer, H., Birk, M., Blom, C., Carli, B., Carlotti, M., von Clarmann, T., Delbouille, L., Dudhia, A., Ehalt, D., Endemann, M., Flaud, J. M.,
9 Gessner, R., Kleinert, A., Koopman, R., Langen, J., López-Puertas, M., Mosner, P., Nett, H., Oelhaf, H., Perron, G., Remedios, J., Ridolfi,
10 M., Stiller, G. P., and Zander, R.: MIPAS: An instrument for atmospheric and climate research, *Atmospheric Chemistry & Physics*, 8,
11 2151 – 2188, <https://doi.org/10.5194/acp-8-2151-2008>, 2008.



- 12 Forster, P. M. d. F. and Shine, K. P.: Assessing the climate impact of trends in stratospheric water vapor, *Geophysical Research Letters*, 29,
13 1086, <https://doi.org/10.1029/2001GL013909>, 2002.
- 14 Fueglistaler, S., Dessler, A. E., Dunkerton, T. J., Folkins, I., Fu, Q., and Mote, P. W.: Tropical tropopause layer, *Reviews of Geophysics*, 47,
15 RG1004, <https://doi.org/10.1029/2008RG000267>, 2009.
- 16 Fujiwara, M., Wright, J. S., Manney, G. L., Gray, L. J., Anstey, J., Birner, T., Davis, S., Gerber, E. P., Harvey, V. L., Heggin, M. I.,
17 Homeyer, C. R., Knox, J. A., Krüger, K., Lambert, A., Long, C. S., Martineau, P., Molod, A., Monge-Sanz, B. M., Santee, M. L., Tegt-
18 meier, S., Chabrillat, S., Tan, D. G. H., Jackson, D. R., Polavarapu, S., Compo, G. P., Dragani, R., Ebisuzaki, W., Harada, Y., Kobayashi,
19 C., McCarty, W., Onogi, K., Pawson, S., Simmons, A., Wargan, K., Whitaker, J. S., and Zou, C.-Z.: Introduction to the SPARC Re-
20 analysis Intercomparison Project (S-RIP) and overview of the reanalysis systems, *Atmospheric Chemistry & Physics*, 17, 1417 – 1452,
21 <https://doi.org/10.5194/acp-17-1417-2017>, 2017.
- 22 Garcia, R. R., Marsh, D. R., Kinnison, D. E., Boville, B. A., and Sassi, F.: Simulation of secular trends in the middle atmosphere, 1950-2003,
23 *Journal of Geophysical Research*, 112, D09 301, <https://doi.org/10.1029/2006JD007485>, 2007.
- 24 Gilford, D. M., Solomon, S., and Portmann, R. W.: Radiative impacts of the 2011 abrupt drops in water vapor and ozone in the tropical
25 tropopause layer, *Journal of Climate*, 29, 595 – 612, <https://doi.org/10.1175/JCLI-D-15-0167.1>, 2016.
- 26 Gille, J. C. and Russell, J. M.: The Limb Infrared Monitor of the Stratosphere – Experiment description, performance, and results, *Journal of*
27 *Geophysical Research*, 89, 5125 – 5140, <https://doi.org/10.1029/JD089iD04p05125>, 1984.
- 28 Hall, E. G., Jordan, A. F., Hurst, D. F., Oltmans, S. J., Vömel, H., Kühnreich, B., and Ebert, V.: Advancements, measurement un-
29 certainties, and recent comparisons of the NOAA frost point hygrometer, *Atmospheric Measurement Techniques*, 9, 4295 – 4310,
30 <https://doi.org/10.5194/amt-9-4295-2016>, 2016.
- 31 Heggin, M. I., Plummer, D. A., Shepherd, T. G., Scinocca, J. F., Anderson, J., Froidevaux, L., Funke, B., Hurst, D., Rozanov, A., Urban,
32 J., von Clarmann, T., Walker, K. A., Wang, H. J., Tegtmeier, S., and Weigel, K.: Vertical structure of stratospheric water vapour trends
33 derived from merged satellite data, *Nature Geoscience*, 7, 768 – 776, <https://doi.org/10.1038/ngeo2236>, 2014.
- 34 Holton, J. R. and Gettelman, A.: Horizontal transport and the dehydration of the stratosphere, *Geophysical Research Letters*, 28, 2799 –
35 2802, <https://doi.org/10.1029/2001GL013148>, 2001.
- 36 Hurrell, J. W., Holland, M. M., Gent, P. R., Ghan, S., Kay, J. E., Kushner, P. J., Lamarque, J.-F., Large, W. G., Lawrence, D., Lindsay, K.,
37 Lipscomb, W. H., Long, M. C., Mahowald, N., Marsh, D. R., Neale, R. B., Rasch, P., Vavrus, S., Vertenstein, M., Bader, D., Collins,
1 W. D., Hack, J. J., Kiehl, J., and Marshall, S.: The Community Earth System Model: A framework for collaborative research, *Bulletin of*
2 *the American Meteorological Society*, 94, 1339 – 1360, <https://doi.org/10.1175/BAMS-D-12-00121.1>, 2013.
- 3 Hurst, D. F., Oltmans, S. J., Vömel, H., Rosenlof, K. H., Davis, S. M., Ray, E. A., Hall, E. G., and Jordan, A. F.: Stratospheric wa-
4 ter vapor trends over Boulder, Colorado: Analysis of the 30 year Boulder record, *Journal of Geophysical Research*, 116, D02 306,
5 <https://doi.org/10.1029/2010JD015065>, 2011.
- 6 Jöckel, P., Kerkweg, A., Pozzer, A., Sander, R., Tost, H., Riede, H., Baumgaertner, A., Gromov, S., and Kern, B.: Development cycle 2 of the
7 Modular Earth Submodel System (MESSy2), *Geoscientific Model Development*, 3, 717 – 752, <https://doi.org/10.5194/gmd-3-717-2010>,
8 2010.
- 9 Jöckel, P., Tost, H., Pozzer, A., Kunze, M., Kirner, O., Brenninkmeijer, C. A. M., Brinkop, S., Cai, D. S., Dyroff, C., Eckstein, J., Frank, F.,
10 Garny, H., Gottschaldt, K.-D., Graf, P., Grewe, V., Kerkweg, A., Kern, B., Matthes, S., Mertens, M., Meul, S., Neumaier, M., Nützel,
11 M., Oberländer-Hayn, S., Ruhnke, R., Runde, T., Sander, R., Scharffe, D., and Zahn, A.: Earth System Chemistry integrated Mod-



- 12 elling (ESCiMo) with the Modular Earth Submodel System (MESSy) version 2.51, *Geoscientific Model Development*, 9, 1153 – 1200,
13 <https://doi.org/10.5194/gmd-9-1153-2016>, 2016.
- 14 Kley, D., Russell, J. M., and Philips, C.: Stratospheric Processes and their Role in Climate (SPARC) - Assessment of upper tropospheric and
15 stratospheric water vapour, SPARC Report 2, WMO/ICSU/IOC World Climate Research Programme, Geneva, 2000.
- 16 Kunz, A., Müller, R., Homonnai, V., Jánosi, I. M., Hurst, D., Rap, A., Forster, P. M., Rohrer, F., Spelten, N., and Riese, M.: Extending
17 water vapor trend observations over Boulder into the tropopause region: Trend uncertainties and resulting radiative forcing, *Journal of*
18 *Geophysical Research*, 118, 11 269 – 11 284, <https://doi.org/10.1002/jgrd.50831>, 2013.
- 19 Livesey, N. J., Read, W. J., Wagner, P. A., Froidevaux, L., Lambert, A., Manney, G. L., Millan, L. F., Pumphrey, H. C., Santee, M. L.,
20 Schwartz, M. J., Wang, S., Fuller, R. A., Jarnot, R. F., Knosp, B. W., , and Martinez, E.: Aura/MLS version 4.2x level 2 data quality and
21 description document, http://mls.jpl.nasa.gov/data/v4-2_data_quality_document.pdf, Last access: 18 August 2017, 2015.
- 22 Lossow, S., Khosrawi, F., Nedoluha, G. E., Azam, F., Bramstedt, K., Burrows, J. P., Dinelli, B. M., Eriksson, P., Espy, P. J., García-Comas,
23 M., Gille, J. C., Kiefer, M., Noël, S., Raspollini, P., Read, W. G., Rosenlof, K. H., Rozanov, A., Sioris, C. E., Stiller, G. P., Walker,
24 K. A., and Weigel, K.: The SPARC water vapour assessment II: comparison of annual, semi-annual and quasi-biennial variations in
25 stratospheric and lower mesospheric water vapour observed from satellites, *Atmospheric Measurement Techniques*, 10, 1111 – 1137,
26 <https://doi.org/10.5194/amt-10-1111-2017>, 2017.
- 27 Marsh, D. R., Mills, M. J., Kinnison, D. E., Lamarque, J.-F., Calvo, N., and Polvani, L. M.: Climate change from 1850 to 2005 simulated in
28 CESM1(WACCM), *Journal of Climate*, 26, 7372 – 7391, <https://doi.org/10.1175/JCLI-D-12-00558.1>, 2013.
- 29 Maycock, A. C., Joshi, M. M., Shine, K. P., Davis, S. M., and Rosenlof, K. H.: The potential impact of changes in lower stratospheric water
30 vapour on stratospheric temperatures over the past 30 years, *Quarterly Journal of the Royal Meteorological Society*, 140, 2176 – 2185,
31 <https://doi.org/10.1002/qj.2287>, 2014.
- 32 McKenna, D. S., Grooß, J.-U., Günther, G., Konopka, P., Müller, R., Carver, G., and Sasano, Y.: A new Chemical Lagrangian Model
33 of the Stratosphere (CLaMS) 2. Formulation of chemistry scheme and initialization, *Journal of Geophysical Research*, 107, 4256,
34 <https://doi.org/10.1029/2000JD000113>, 2002a.
- 35 McKenna, D. S., Konopka, P., Grooß, J.-U., Günther, G., Müller, R., Spang, R., Offermann, D., and Orsolini, Y.: A new Chemical La-
36 grangian Model of the Stratosphere (CLaMS) 1. Formulation of advection and mixing, *Journal of Geophysical Research*, 107, 4309,
37 <https://doi.org/10.1029/2000JD000114>, 2002b.
- 1 McLandress, C., Scinocca, J. F., Shepherd, T. G., Reader, M. C., and Manney, G. L.: Dynamical control of the mesosphere by orographic
2 and nonorographic gravity wave drag during the extended northern winters of 2006 and 2009, *Journal of the Atmospheric Sciences*, 70,
3 2152 – 2169, <https://doi.org/10.1175/JAS-D-12-0297.1>, 2013.
- 4 McLandress, C., Plummer, D. A., and Shepherd, T. G.: Technical Note: A simple procedure for removing temporal discontinuities in ERA-
5 Interim upper stratospheric temperatures for use in nudged chemistry-climate model simulations, *Atmospheric Chemistry & Physics*, pp.
6 1547 – 1555, <https://doi.org/10.5194/acp-14-1547-2014>, 2014.
- 7 Moyer, E. J., Irion, F. W., Yung, Y. L., and Gunson, M. R.: ATMOS stratospheric deuterated water and implications for troposphere-
8 stratosphere transport, *Geophysical Research Letters*, 23, 2385 – 2388, <https://doi.org/10.1029/96GL01489>, 1996.
- 9 Notholt, J., Toon, G. C., Fueglistaler, S., Wennberg, P. O., Irion, F. W., McCarthy, M., Scharringhausen, M., Siek Rhee, T., Kleinböhl, A.,
10 and Velasco, V.: Trend in ice moistening the stratosphere - constraints from isotope data of water and methane, *Atmospheric Chemistry*
11 *& Physics*, 10, 201 – 207, <https://doi.org/10.5194/acp-10-201-2010>, 2010.



- 12 Oltmans, S. J. and Hofmann, D. J.: Increase in lower-stratospheric water vapour at a mid-latitude Northern Hemisphere site from 1981 to
13 1994, *Nature*, 374, 146 – 149, <https://doi.org/10.1038/374146a0>, 1995.
- 14 Oltmans, S. J., Vömel, H., Hofmann, D. J., Rosenlof, K. H., and Kley, D.: The increase in stratospheric water vapor from balloonborne,
15 frostpoint hygrometer measurements at Washington, D.C., and Boulder, Colorado, *Geophysical Research Letters*, 27, 3453 – 3456,
16 <https://doi.org/10.1029/2000GL012133>, 2000.
- 17 Ploeger, F., Günther, G., Konopka, P., Fueglistaler, S., Müller, R., Hoppe, C., Kunz, A., Spang, R., Groß, J.-U., and Riese, M.: Horizontal
18 water vapor transport in the lower stratosphere from subtropics to high latitudes during boreal summer, *Journal of Geophysical Research*,
19 118, 8111 – 8127, <https://doi.org/10.1002/jgrd.50636>, 2013.
- 20 Randel, W. J., Wu, F., Vömel, H., Nedoluha, G. E., and Forster, P.: Decreases in stratospheric water vapor after 2001: Links
21 to changes in the tropical tropopause and the Brewer-Dobson circulation, *Journal of Geophysical Research*, 111, D12 312,
22 <https://doi.org/10.1029/2005JD006744>, 2006.
- 23 Randel, W. J., Polvani, L., Wu, F., Kinnison, D. E., Zou, C., and Mears, C.: Troposphere-stratosphere temperature trends de-
24 rived from satellite data compared with ensemble simulations from WACCM, *Journal of Geophysical Research*, 122, 1 – 17,
25 <https://doi.org/10.1002/2017JD027158>, 2017.
- 26 Rienecker, M. M., Suarez, M. J., Gelaro, R., Todling, R., Bacmeister, J., Liu, E., Bosilovich, M. G., Schubert, S. D., Takacs, L., Kim, G.-K.,
27 Bloom, S., Chen, J., Collins, D., Conaty, A., da Silva, A., Gu, W., Joiner, J., Koster, R. D., Lucchesi, R., Molod, A., Owens, T., Pawson, S.,
28 Pegion, P., Redder, C. R., Reichle, R., Robertson, F. R., Ruddick, A. G., Sienkiewicz, M., and Woollen, J.: MERRA: NASA's Modern-Era
29 Retrospective Analysis for Research and Applications, *Journal of Climate*, 24, 3624 – 3648, <https://doi.org/10.1175/JCLI-D-11-00015.1>,
30 2011.
- 31 Riese, M., Ploeger, F., Rap, A., Vogel, B., Konopka, P., Dameris, M., and Forster, P.: Impact of uncertainties in atmo-
32 spheric mixing on simulated UTLS composition and related radiative effects, *Journal of Geophysical Research*, 117, D16 305,
33 <https://doi.org/10.1029/2012JD017751>, 2012.
- 34 Roeckner, E., Brokopf, R., Esch, M., Giorgetta, M., Hagemann, S., Kornbluh, L., Manzini, E., Schlese, U., and Schulzweida, U.: Sensi-
35 tivity of Simulated Climate to Horizontal and Vertical Resolution in the ECHAM5 Atmosphere Model, *Journal of Climate*, 19, 3771,
36 <https://doi.org/10.1175/JCLI3824.1>, 2006.
- 37 Rosenlof, K. H. and Reid, G. C.: Trends in the temperature and water vapor content of the tropical lower stratosphere: Sea surface connection,
38 *Journal of Geophysical Research*, 113, D06 107, <https://doi.org/10.1029/2007JD009109>, 2008.
- 1 Scherer, M., Vömel, H., Fueglistaler, S., Oltmans, S. J., and Staehelin, J.: Trends and variability of midlatitude stratospheric water
2 vapour deduced from the re-evaluated Boulder balloon series and HALOE, *Atmospheric Chemistry & Physics*, 8, 1391 – 1402,
3 <https://doi.org/10.5194/acp-8-1391-2008>, 2008.
- 4 Schieferdecker, T., Lossow, S., Stiller, G. P., and von Clarmann, T.: Is there a solar signal in lower stratospheric water vapour?, *Atmospheric*
5 *Chemistry & Physics*, 15, 9851 – 9863, <https://doi.org/10.5194/acp-15-9851-2015>, 2015.
- 6 Scinocca, J. F., McFarlane, N. A., Lazare, M., Li, J., and Plummer, D.: Technical Note: The CCCma third generation AGCM and its extension
7 into the middle atmosphere, *Atmospheric Chemistry & Physics*, 8, 7055 – 7074, 2008.
- 8 Solomon, S.: Stratospheric ozone depletion: A review of concepts and history, *Reviews of Geophysics*, 37, 275 – 316,
9 <https://doi.org/10.1029/1999RG900008>, 1999.
- 10 Solomon, S., Rosenlof, K. H., Portmann, R. W., Daniel, J. S., Davis, S. M., Sanford, T. J., and Plattner, G.: Contributions of stratospheric
11 water vapor to decadal changes in the rate of global warming, *Science*, 327, 1219 – 1223, <https://doi.org/10.1126/science.1182488>, 2010.



- 12 Stenke, A. and Grewe, V.: Simulation of stratospheric water vapor trends: impact on stratospheric ozone chemistry, *Atmospheric Chemistry*
13 *& Physics*, 5, 1257 – 1272, 2005.
- 14 Stiller, G. P., von Clarmann, T., Haedel, F., Funke, B., Glatthor, N., Grabowski, U., Kellmann, S., Kiefer, M., Linden, A., Lossow, S.,
15 and López-Puertas, M.: Observed temporal evolution of global mean age of stratospheric air for the 2002 to 2010 period, *Atmospheric*
16 *Chemistry & Physics*, 12, 3311 – 3331, <https://doi.org/10.5194/acp-12-3311-2012>, 2012.
- 17 Uppala, S. M., Kållberg, P. W., Simmons, A. J., Andrae, U., Bechtold, V. D. C., Fiorino, M., Gibson, J. K., Haseler, J., Hernandez, A., Kelly,
18 G. A., Li, X., Onogi, K., Saarinen, S., Sokka, N., Allan, R. P., Andersson, E., Arpe, K., Balmaseda, M. A., Beljaars, A. C. M., Berg,
19 L. V. D., Bidlot, J., Bormann, N., Caires, S., Chevallier, F., Dethof, A., Dragosavac, M., Fisher, M., Fuentes, M., Hagemann, S., Hólm,
20 E., Hoskins, B. J., Isaksen, I., Janssen, P. A. E. M., Jenne, R., McNally, A. P., Mahfouf, J.-F., Morcrette, J.-J., Rayner, N. A., Saunders,
21 R. W., Simon, P., Sterl, A., Trenberth, K. E., Untch, A., Vasiljevic, D., Viterbo, P., and Woollen, J.: The ERA-40 re-analysis, *Quarterly*
22 *Journal of the Royal Meteorological Society*, 131, 2961 – 3012, <https://doi.org/10.1256/qj.04.176>, 2005.
- 23 Vömel, H., David, D. E., and Smith, K.: Accuracy of tropospheric and stratospheric water vapor measurements by the
748 cryogenic frost point hygrometer: Instrumental details and observations, *Journal of Geophysical Research*, 112, D08 305,
749 <https://doi.org/10.1029/2006JD007224>, 2007.
- 750 von Clarmann, T., Stiller, G., Grabowski, U., Eckert, E., and Orphal, J.: Technical Note: Trend estimation from irregularly sampled, correlated
751 data, *Atmospheric Chemistry & Physics*, 10, 6737 – 6747, 2010.
- 752 Waters, J. W., Froidevaux, L., Harwood, R. S., Jarnot, R. F., Pickett, H. M., Read, W. G., Siegel, P. H., Cofield, R. E., Filipiak, M. J., Flower,
753 D. A., Holden, J. R., Lau, G. K., Livesey, N. J., Manney, G. L., Pumphrey, H. C., Santee, M. L., Wu, D. L., Cuddy, D. T., Lay, R. R., Loo,
754 M. S., Perun, V. S., Schwartz, M. J., Stek, P. C., Thurstans, R. P., Boyles, M. A., Chandra, K. M., Chavez, M. C., Chen, G.-S., Chudasama,
755 B. V., Dodge, R., Fuller, R. A., Girard, M. A., Jiang, J. H., Jiang, Y., Knosp, B. W., Labelle, R. C., Lam, J. C., Lee, A. K., Miller, D.,
756 Oswald, J. E., Patel, N. C., Pukala, D. M., Quintero, O., Scaff, D. M., Vansnyder, W., Tope, M. C., Wagner, P. A., and Walch, M. J.:
757 The Earth Observing System Microwave Limb Sounder (EOS MLS) on the Aura Satellite, *IEEE Transactions on Geoscience and Remote*
758 *Sensing*, 44, 1075 – 1092, <https://doi.org/10.1109/TGRS.2006.873771>, 2006.

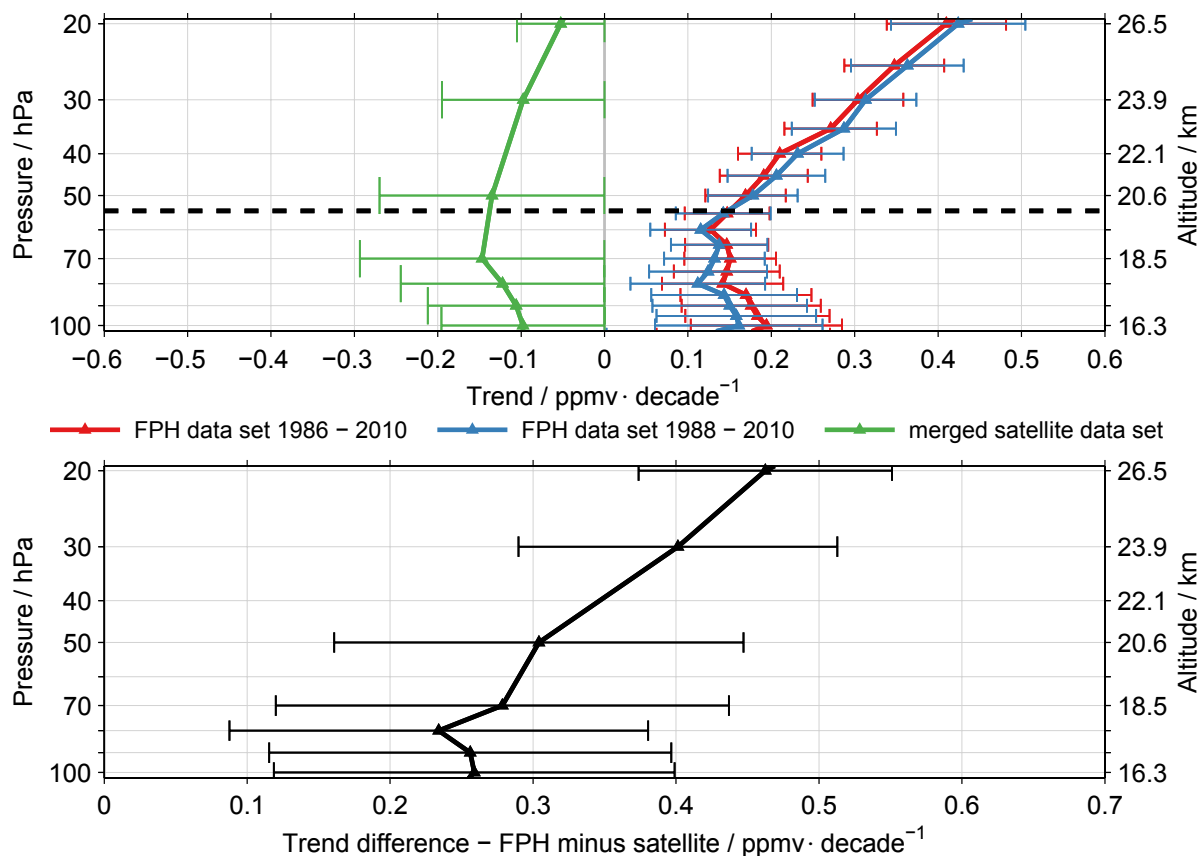


Figure 1. Upper panel: In green the approximated trend estimates derived from the merged satellite data set for the the latitude band between 35°N and 45°N are shown. See text for more details. Below the dashed line these estimates consider the time period from 1988 to 2010, above they are for the time period from 1986 to 2010. In red and blue the corresponding trend estimates derived from the FPH observations at Boulder are shown. The error bars represent the 2σ uncertainty. The right axis provides an approximation of the altitude in geometrical terms. This information is derived from the MIPAS data. Lower panel: Difference between the trend estimates derived from the FPH observations and merged satellite data set.

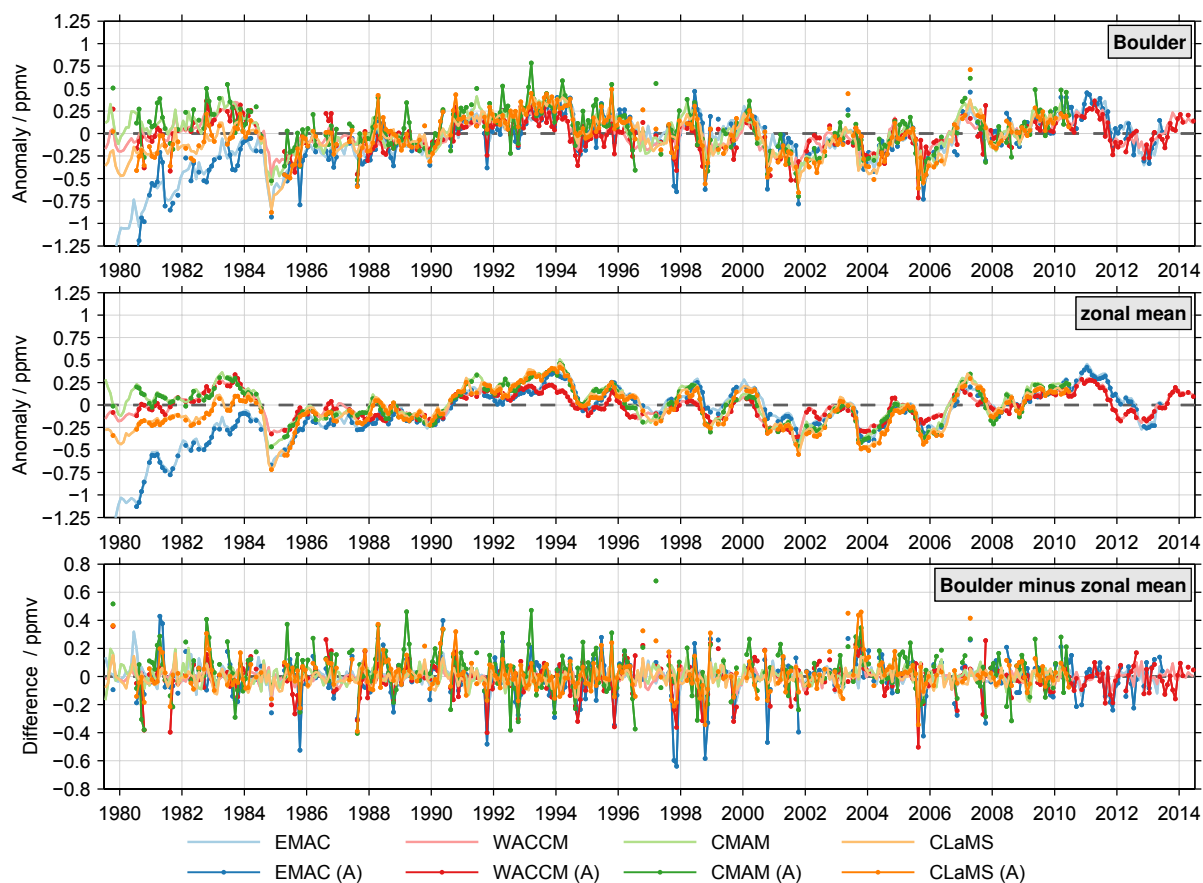


Figure 2. De-seasonalised time series for Boulder (top panel), the 35°N to 45°N zonal mean (middle panel) and its difference (low panel) for a number of model simulations considering the pressure level of 70 hPa. Results labelled with the suffix (A) are adapted to the actual FPH observations at Boulder, see text for more details. The time ticks consider the middle of the specified years.

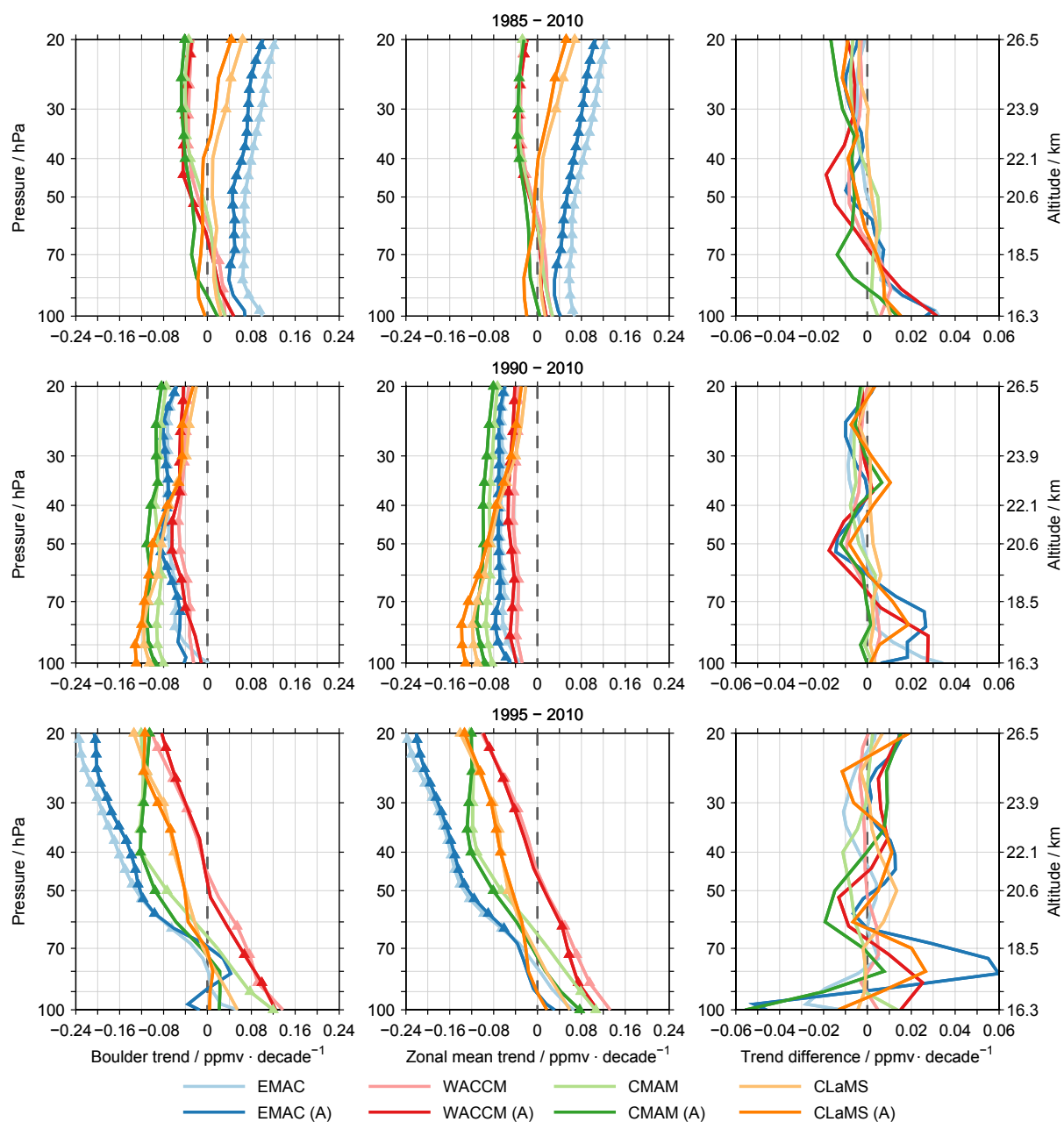


Figure 3. Trend estimates for the different model simulations for Boulder (left panels), the zonal mean for the latitude band between 35°N and 45°N (centre panels) and their corresponding differences (right panels). The different rows consider different time period as indicated in the title of the centre panels. Trends and trend differences significant at the 2σ uncertainty level are marked by triangles.

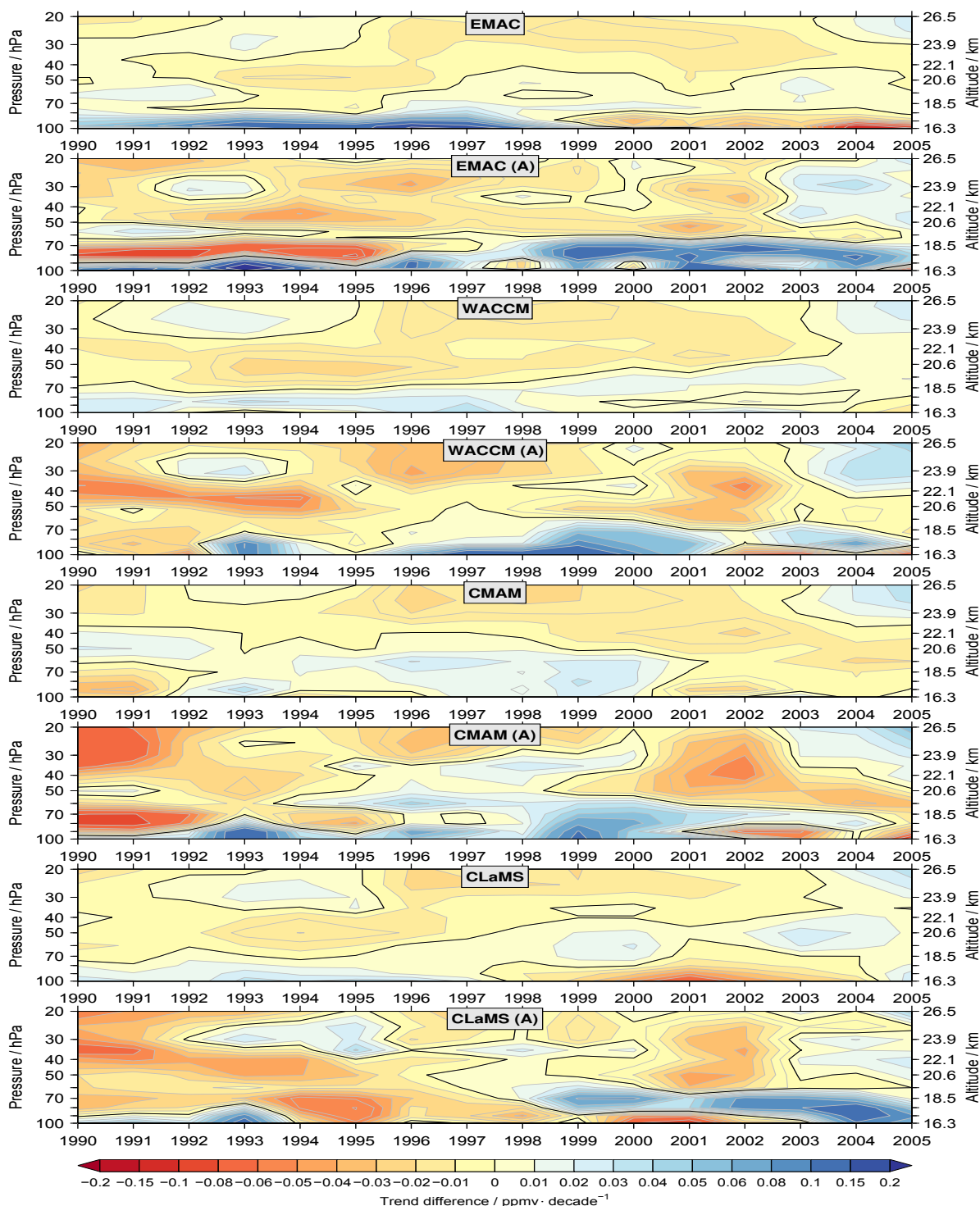


Figure 4. The temporal development of the trend differences between the Boulder and the zonal mean ($35^{\circ}\text{N} - 45^{\circ}\text{N}$) time series, based on 11 year time intervals. The results are given at the centre of the corresponding time intervals, i.e. in 1995 for the time period between 1990 and 2000. The black lines indicate zero trend differences.

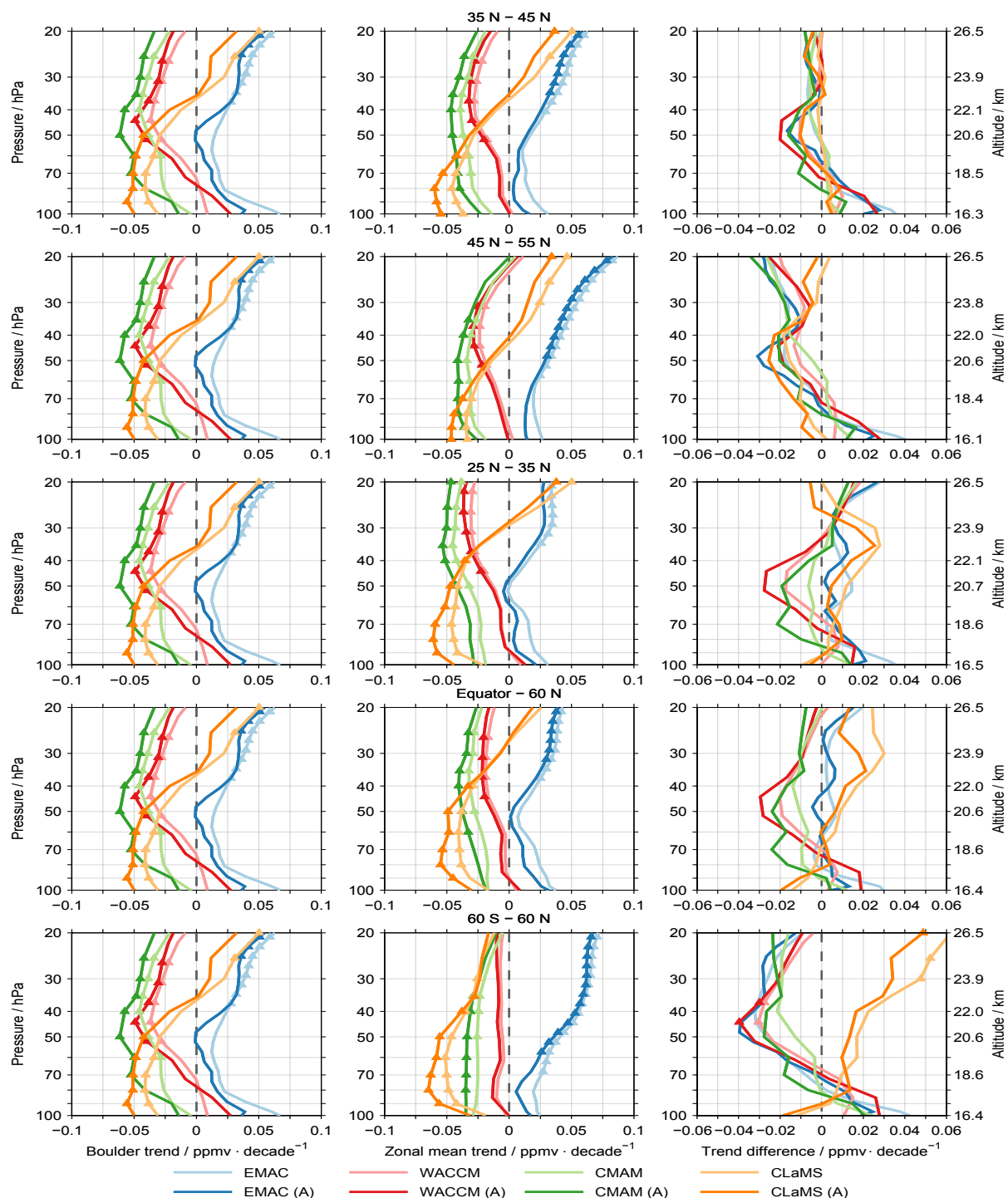


Figure 5. Comparison of the trend estimates at Boulder (left panels) and the zonal means for different latitude bands (centre panels) as indicated in the title. As in Fig. 3 the right panels show the difference between the two trends. The comparisons consider the time period between 1987 and 2010. The left panels are all the same and are repeated for convenience.

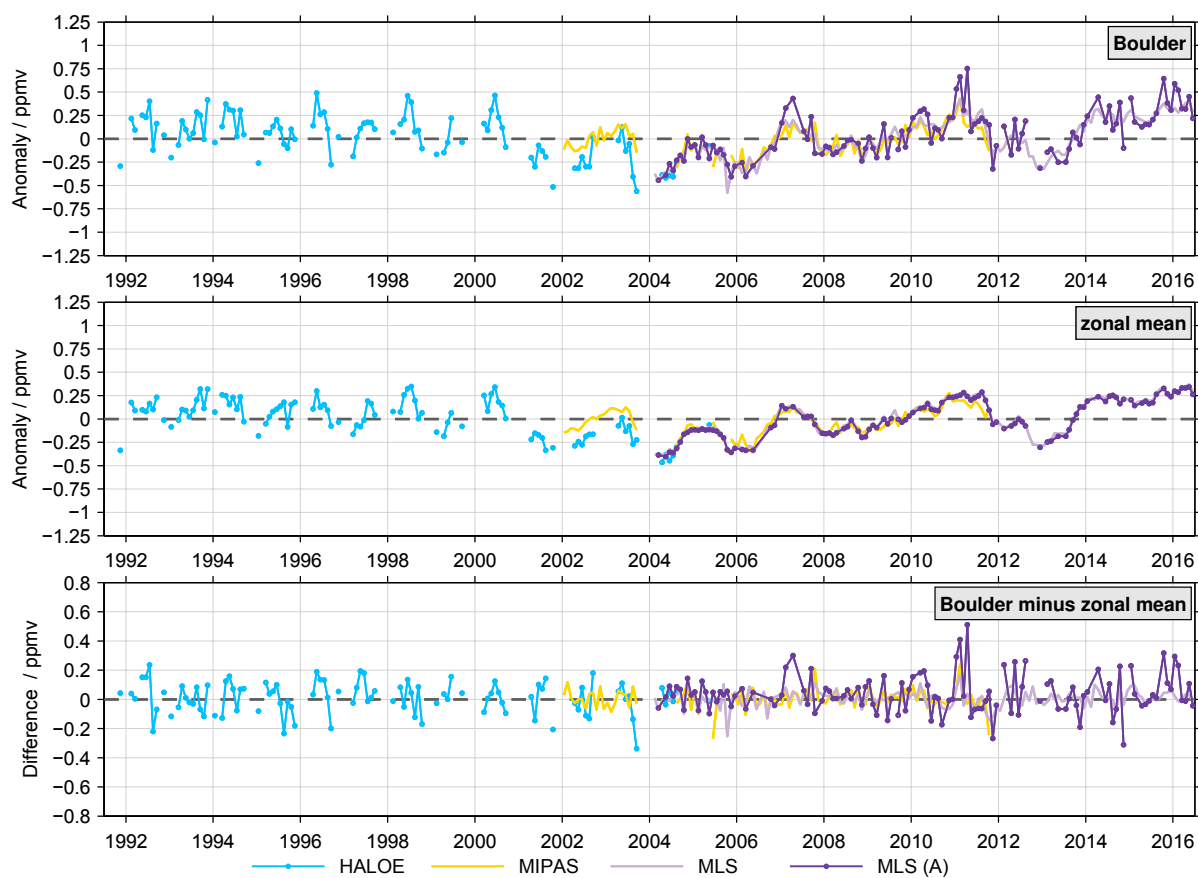


Figure 6. As Fig. 2 but here showing several observational results.

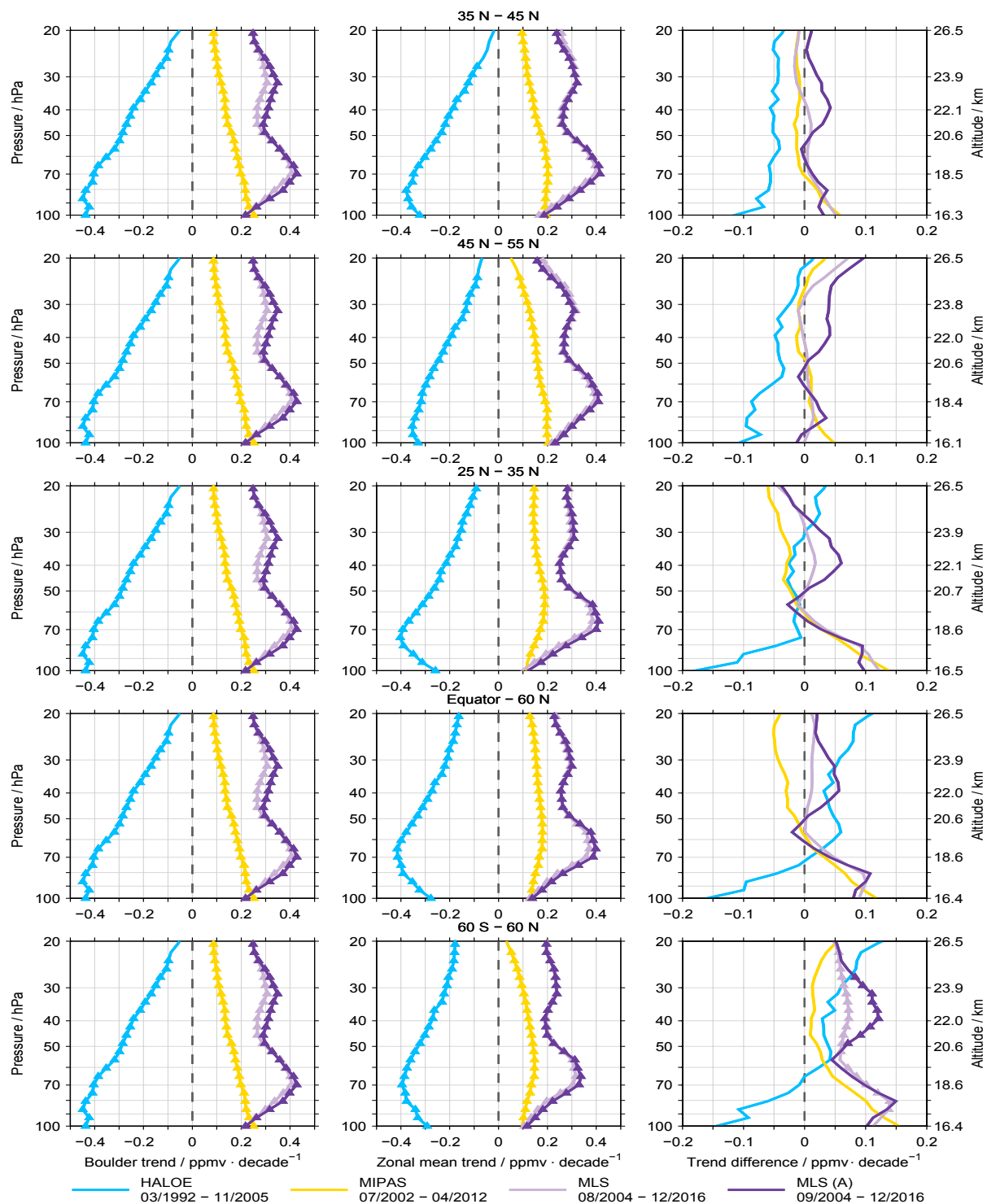


Figure 7. As Fig. 5 but here again for the observations.

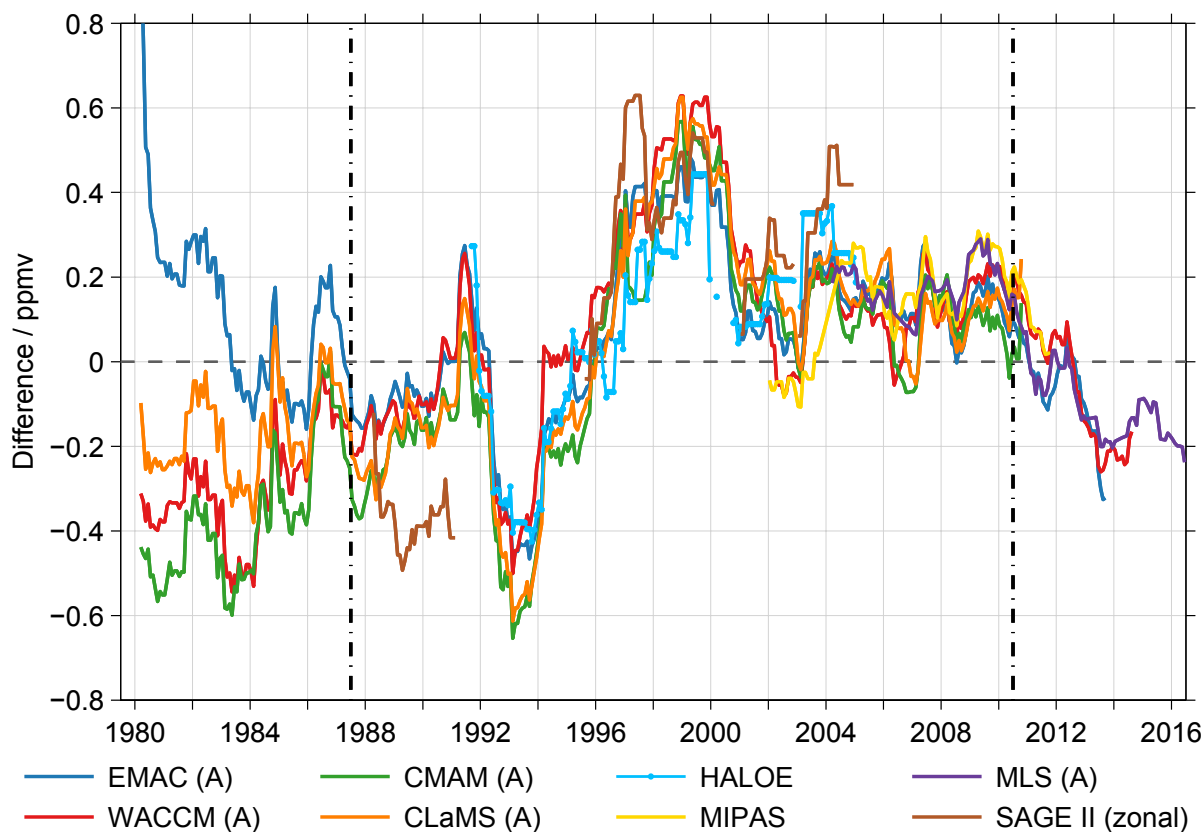


Figure 8. Differences between the de-seasonalised time series obtained from the FPH observations and the Boulder time series derived from the different simulations and observational results at 70 hPa. To provide a clearer picture, the differences are smoothed with a 1 year running average. At least three data points are required for a valid running average. The dashed-dotted line indicates the time period covered by the merged satellite data set. The time ticks consider again the middle of the specified years.